Universitetet i Stavanger

FACULTY OF SCIENCE AND TECHNOLOGY

MASTER'S THESIS

Study program/specialization: Master of Science in Energy & Petroleum Engineering/ Drilling Engineering	Spring semester, 2023. Open access
Author: Pedram K.Gargari	*Pedram K. Gargari* (Author's signature)
Supervisor(s): Prof. Mahmoud Khalifeh Dr. Reidar Inge Korsnes	
Title of master's thesis: Investigating the Necessity of Standardized In-Situ Testing Procedures for One-Part Granite-based Geopolymers: Examining the Impact of Temperature and Confining Pressure through Experimental Study	
Credits: 30 ECTS	
Keywords: Geopolymer In-situ mechanical properties Bulk modulus Yield strength Young's modulus	Number of pages: 68 Stavanger, 15th June 2023

Investigating the Necessity of Standardized In-Situ Testing Procedures for One-Part Granite-based Geopolymers: Examining the Impact of Temperature and Confining Pressure through Experimental Study

By

Pedram K.Gargari

Master's Thesis

Presented to the Faculty of Science and Technology at The University of Stavanger

THE UNIVERSITY OF STAVANGER JUNE 2023

Acknowledgment

I want to express my special thanks to my supervisors at the University of Stavanger, Prof. Mahmoud Khalifeh, and Dr. Reidar Inge Korsnes, who gave me the opportunity, provided me with this project and motivated me through it. I also want to thank Ph.D. candidates Seyed Hasan Hajiabadi and Mohamed Omran for their guidance and counseling throughout the project.

I also acknowledge the Research Council of Norway (RCN) for financing the Centre for Research-based Innovation "SWIPA - Centre for Subsurface Well Integrity, Plugging and Abandonment," RCN proj. no. 309646, for which the work has been partially carried out.

Lastly, I gratefully acknowledge TotalEnergies, AkerBP, ConocoPhillips, and the Research Council of Norway for financially supporting the SafeRock KPN Project (RCN #319014) at the University of Stavanger, Norway.

At last, I would like to thank my family and friends for supporting me through my thesis.

Pedram K.Gargari

Stavanger, Spring 2023

Abstract

Ordinary Portland cement (OPC) is widely used in primary cementing and plug and abandonment operations due to its well-known properties, global availability, and affordability. However, it has limitations and durability concerns in corrosive downhole environments. Additionally, OPC contributes significantly to global CO2 emissions (6-8 wt.%). Consequently, industries are exploring alternative cementitious materials that offer comparable or superior fluid-state and physical properties while being more economically viable and environmentally sustainable.

Geopolymer cement (GPC) is an inorganic polymer with binding properties, forming a 3D network structure of silicate and aluminum. GPC exhibits stability at high temperatures, increased durability in corrosive environments, greater flexibility, and lower matrix permeability compared to OPC. Although these advantages make GPC an excellent alternative to OPC, its application in oilfields is still limited to laboratory-scale experiments due to the young age of the technology.

This study is complementary to two other projects being conducted to reveal the potential necessity of standard procedures for testing in-situ rock mechanical properties of the GPC. Since the impact of pore pressure and loading rate is covered in the other two projects, this work presents the effect of temperature and confining pressure on the in-situ mechanical properties of the one-part granite-based geopolymer cement. A triaxial cell is used to analyze Young's modulus, bulk modulus, Poisson's ratio, and compressive strength of the material at three different temperatures and confining pressure.

The GPC sample preparation procedure is optimized during the study after experiencing inconsistent and unreliable results during the first seven tests. The increase in test temperature resulted in a decrease in yield strength, peak stress, and Young's modulus while causing an increase in the bulk modulus. The sensitivity of the material to temperature decreases with the increase of confining pressure. The increase in confining pressure also increased yield strength and peak stress of the material.

Acronyms

˚C	Degree of Celcius
CO2	Carbon Di-oxide
GGBFS	Ground Granulated Blast-furnace Slag
GPC	Geopolymer Cement
GPa	Gigapascal
MPa	Megapascal
OPC	Ordinary Portland Cement
Wt.%	Weight Percentage

Table of Content

List of Figures

List of Tables

1 Introduction

When a well has produced all its potential and has reached to end of its lifetime, it must be permanently plugged and abandoned, also known as a permanent P&A operation. Many other occasions, such as sidetracking for bypassing, slot recovery, well integrity issues, re-development, and abandoning dry holes, are reasons permanent P&A operation is undergone. The objective of one P&A operation is to repair the drilled cap-rock and restore its functionality, resulting in a well with permanent secured well integrity. To obtain this objective, a set of actions and tasks must be taken to protect and isolate surroundings, freshwater zones, and the environment from a source of potential inflow. In this case, the potential inflow can include hydrocarbon-bearing zones and water from permeable formations. The presented information in the P&A part of the introduction is based on the book "Introduction to Permanent Plug and Abandonment of Wells" by Mahmoud Khalifeh and Arild Saasen.[1]

Different definitions exist of the term "well integrity"; NORSOK D-010 defines well-integrity as "the application of technical, operational and organizational solutions to reduce risk of uncontrolled release of formation fluids and well fluids throughout the well's lifecycle." The requirements, commitments, and responsibilities that are necessary to maintain well integrity is known as well integrity management systems (WIMS), which have been a great solution for organizations to ensure the safeguarding of safety, health, environment, and assets while managing the risk of loss of well containment.

To maintain well integrity, sufficient well barriers should be established to prevent any uncontrolled flows. In other words, two independent barriers should be established where the second barrier (secondary barrier) acts as a backup to the first barrier (primary barrier) and is therefore not engaged unless the primary barrier fails. This theory is also known as the "hat-over-hat" principle or two-barrier philosophy, which has been employed since the 1920s. With technological improvements, the petroleum industry has entered more challenging and complex environments. This has been followed up with an increase in standardizing well barrier integrity and complicity of the two-barrier philosophy.

A plug is a device or an object that is placed in the wellbore with the intention of blocking the passageway. Plugs are divided into two groups based on the engineering context:

- Mechanical plugs
- Non-mechanical plugs.

Mechanical plugs are not accepted as part of the permanent well barrier envelope when considering permanent well abandonment. The specific reason for that is concerns regarding its long-term durability in the deep and rough environment of a wellbore. Nevertheless, mechanical plugs are used as a foundation or base for placing the non-mechanical plug on top of it. A non-mechanical plug is a sealing object placed in the wellbore and is usually a setting material. They are mostly used in permanent P&A operations combined with bridge plugs (cased holes) or viscous pills (Open holes). Using bridge plugs (mechanical plugs) as a foundation is a common method to reduce the risk of contamination and ensure the correct placement of the material. For a setting material to be accepted as a permanent well barrier envelope, it must fulfill several functional requirements such as bonding properties, sealing capability, durability, downhole placeability, and reparability. Portland cement is the most known and studied setting material that fulfills most of the mentioned requirements.[2]. Perhaps one could claim the outlined functional requirements are deducted from the chemical and physical properties of OPC; thus, it fulfills these requirements.

1.1 Portland Cement

Portland cement is the most known setting material introduced by Joseph Aspdin in 1824 and has had an important role in the petroleum industry. Portland cement is produced when a material with a high concentration of calcium carbonate, such as limestone, is calcined with shale or clay at 1500 °C. Following calcination, clinkers are produced after a partial fusion. The cement production is finalized by adding a few percent of gypsum to the clinkers, and the mixture is finally finely grounded. The gypsum in the mix acts as a setting rate controller and can be replaced by other materials containing calcium sulfate. The component of clinkers in normal Portland cement is presented in Table 1.1.

Table 1.1 - Component of Portland cement clinkers

Component	wt.%
CaO	67
SiO_2	22
Al_2O_3	5
Fe_2O_3	3
Others	3

Adding water to the cement initiates a reaction involving the hydration of di- and tri-calcium silicates, and tricalcium aluminate, leading to the production of calcium silicate hydrate, lime, and heat. These reactions result in the creation of C-S-H fiber structures, also known as CASH networks which are crucial contributors to the strength development of cement paste. Eq 1.1 presents the mentioned reaction where ΔH is assumed as enthalpy. [2]

$$2C_3S + 6H2O \rightarrow C_3S_2H_3 + 3CH, \Delta H = 120 \text{ cal/g} \quad (1.1)$$

As mentioned, Portland cement has had a crucial role in the petroleum industry as a setting material for primary cementing and P&A operations however, following the recent restrictions and global warming concerns, its shortcoming has gotten more noticeable. Portland cement consumes a large amount of energy during the calcination of the limestone process, which leads to large emissions of carbon dioxide (CO_2), nitrogen oxide (NO), and sulfur trioxide (SO_3). Approximately 1500 million tons of cement are produced yearly worldwide, and one metric ton of ordinary Portland cement produces between 0.73 – 0.85 tons of CO_2.[3] In addition, the high calcium concentration in the cement mixture causes poor long-term durability of the setting material in a wellbore environment when exposed to high temperatures and downhole chemicals. To minimize CO_2 emission and energy consumption and reduce well integrity incidents, investigations are ongoing for greener setting material to replace Portland cement while improving its mechanical properties. As a result, geopolymer cement has received great interest from researchers and industries.

1.2 Geopolymer

Geopolymer is an inorganic polymer and a cementitious material class known as a great alternative to ordinary Portland cement. Geopolymer was introduced by Joseph Davidovits in 1978, and several studies have undergone since to optimize and commercialize the technology. Geopolymer cement (GPC) stands out from other OPC alternatives with its low calcium concentration (in some cases under 15 wt.%). Besides its impressive low calcium concentration, studies have shown great long-term durability, compressive strength, and resistance against highly corrosive environments. The binder used to create GPC is rich in aluminum and silicates, allowing industrial waste as the main raw material, making it a great sustainable alternative for OPC while having improvement of mechanical properties. [4-6]

1.2.1 Raw Material - Precursor

The materials that can be used as the solid phase of a geopolymer mixture is known as geopolymer precursor. The precursor consists of a binder (raw material) rich in aluminum and silicates, making it eligible to produce geopolymer. Industrial waste, general waste (recycled waste), and natural materials are three raw materials with different characteristics, availability, application, and cost. There has been some investigation on the mechanical strength of the various raw materials. They concluded that industrial waste has the highest mechanical strength among the other two types of raw materials. Many industrial waste alternatives can be used as the raw material, including clays, fly ash, slag, rice husk ash, natural rocks, and zeolite.

To optimize the chemical composition of precursors, other raw materials can be introduced to the precursor, such as micro-silica and ground granulated blast-furnace slag (GGBFS). Micro-silica, also known as silica fume, is a common additive to the precursor. It acts as a filler and reduces the material's porosity, improving the strength and durability of the GPC.[7] Adding GGBFS, a by-product from the iron and steel industry, provides a great early strength improvement due to its amorphous content and reactive calcium, magnesium, silicate, and aluminate compounds.[8]

1.2.2 Alkali Activator

The activator is the component mainly responsible for the dissolution of the minerals and activating the initial mechanism of geopolymerization. The activation is done by dissolving silica and alumina from the precursor. In addition, when the activator contains silicate species, it plays a role in the geopolymerization of the aluminosilicate species present in the solution by creating long repeating chains of molecules made up of Si-O-Al-O bonds. The activator can be introduced to the mixture as a liquid or solid powder. Geopolymer mixtures with its activator as a solid phase are known as one-part or just add water systems and have a similar preparation method as Portland cement. There are different types of activators; however, the most common are sodium- or potassium silicate and sodium- or potassium hydroxide. Using a potassium-based activator can result in the creation of K-A-S-H gels and, on the other hand, N-A-S-H gels when the sodium-based activator is taken into use. These gels are not geopolymers but an intermediate structure to have the geopolymers. [4]

1.2.3 Curing Temperature

Curing and conditioning temperature are parameters that highly affect the mechanical properties of GPC. Based on a previous study done by Andi Arham Adam et al. (2014), the compressive strength of a fly ash-based geopolymer was at its highest when cured under 120°C compared to 100°C and 80°C. The specimen cured at 80°C had a maximum compressive strength of 19 MPa after seven days, whereas on the other hand, the core cured at 120°C reached the compressive strength of 32 MPa after seven days.[9] Pavel Rovnaník et al. (2009) also observed the same trend when evaluating the effect of curing temperature on metakaolin-based geopolymer. Both early-age and final mechanical properties of geopolymer material depended on curing temperature, and higher curing temperatures increased flexural strength and early-age compressive strength. [10]

1.2.4 Curing Duration

Curing time is an important factor in analyzing cementitious material. Previous studies have confirmed that the curing time of GPC has a crucial effect on the material's mechanical properties. Geopolymer is a cementitious material that has a long-lasting strength development process. Based on studies done by Khalifeh et al. (2016) on rock-based geopolymer, an increase in uniaxial compressive strength has been observed until one year of curing.[11] The most strength development for fly-ash-based geopolymer was observed after seven days according to studies by Andi Arham Adam et al. (2014).[9] Following the internal studies done at the University of Stavanger on the activation of the raw material used in the geopolymer mixture, it has confirmed the optimal time to analyze the material's mechanical properties to be after one week of curing.

1.3 Rock Mechanics

Underground formations are continuously under a state of stress due to tectonic and overburden stresses. After a well is drilled in the formation, the solid materials which were under stress are removed. Hence, the borehole wall is only supported by pressured fluid pumped into the hole, and since the fluid is not able to match the in-situ stresses from the formation, stress around the well is expected. This will also conclude that the casing, primary cement, and the permanent barrier will also experience stresses from the formation. Therefore, understanding rock mechanics is important to discuss and solve the well’s problems. This chapter defines the present stresses and strains in the borehole and analyzes the failure mechanics. Presented information in chapter 1.3 of rock mechanics is based on the book

"Petroleum Related Rock Mechanics" by Fjar, Erling; Holt, R.M.; Raaen, A.M.; Risnes, R.; Horsrud, P. [12]

1.3.1 Stress

Stress is a parameter used to measure the pressure and force applied to a core. The stress is applied to the sample through the axial load and the confining pressure, leading the sample to experience lateral and axial stresses and undergo deformation. Stress (σ) is defined as the force (F) acting on a cross-section area (A), as shown in Eq 1.2. The sum of the axial stress and the confining pressure applied through the confining fluid determines the direction and magnitude of the total stress applied to the core. Total stress is the sum of effective stress and pore water pressure which are crucial parameters for determining the deformation and shear strength of the material.

$$\sigma = \frac{F}{A} = \frac{Force}{Area} \qquad (1.2)$$

1.3.2 Strain

Strain (ε) is the amount of deformation experienced by a sample due to applied external stresses or forces. It is defined as the ratio of the material's dimension change (ΔD) to its original dimension (D), as shown in equation 1.3. The magnitude of deformations, such as compression, stretching, and bending caused by stresses objected to a sample, is measured as strain. This measurement can provide valuable information in engineering about the stiffness, strength, and elasticity of a material, which is important for designing a reliable well barrier element.

$$\varepsilon = \frac{\Delta D}{D} = \frac{Change\ in\ dimension}{Original\ dimension} \quad (1.3)$$

During a triaxial test, the core is subjected to both confining pressure and axial load, causing the sample to experience radial and axial strain and undergo deformation. The change in length of the core along its axial direction is defined as the axial strain, and the change in diameter or circumference of the sample is defined as the radial strain. The strain is typically measured by using a strain gauge or a displacement sensor attached to the core or the loading plates of the triaxial cell.

1.3.3 Yield Strength

Yield strength is defined as the load or stress a material can withstand before it is deformed plastically. Yield strength is an important mechanical property representing the safe working stress or loads a material can endure without permanent deformation. It is determined by measuring the stress and strain of the material during triaxial testing and making a yield point. The yield point is the point on a stress-strain curve that indicates the elastic behavior limit and the start of the plastic behavior of the material. In some materials with a gradual onset of nonlinear behavior, making a precise yield point on the curve is challenging. Therefore, in this study, both 0.2% offset yield point (proof stress) and maximum peak stress is taken into use to analyse strength of the sample. Figure 1.1 presents how the 0.2% offset yield strength is determined in this study.

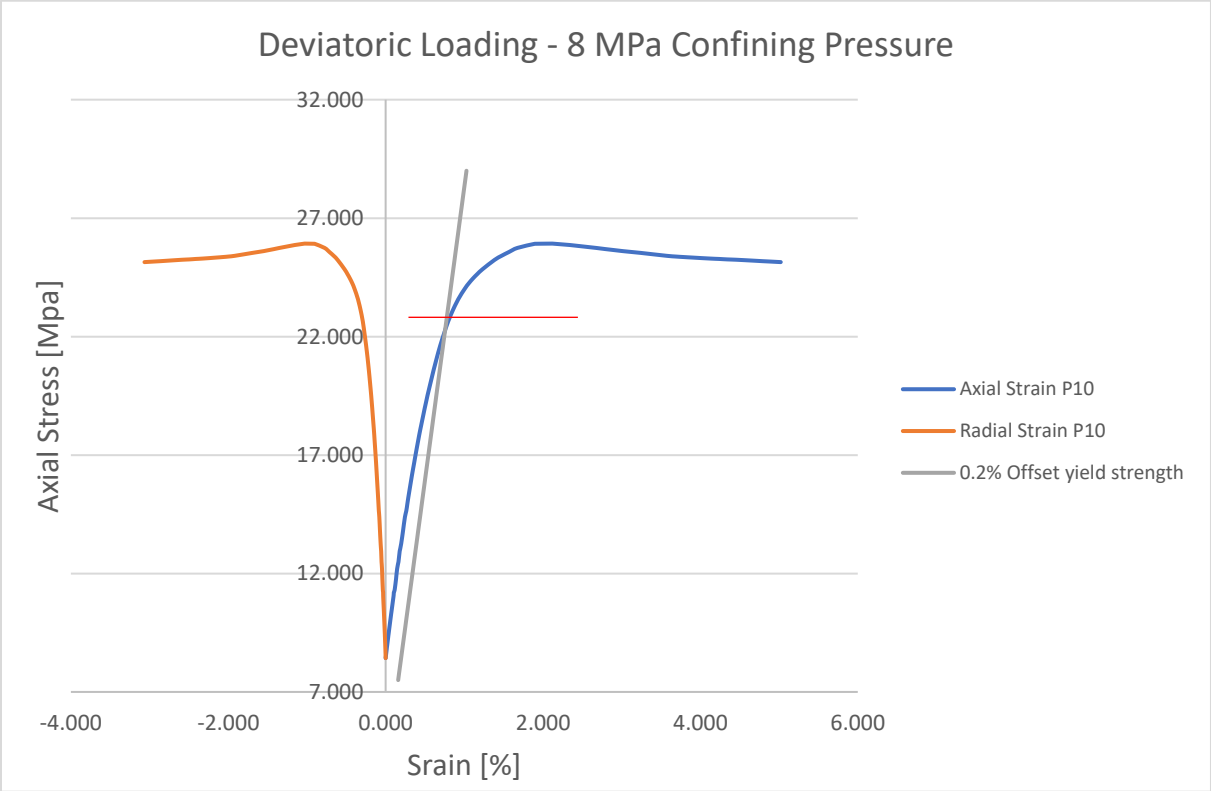

Figure 1.1- 0.2% offset yield strength

1.3.4 Bulk Modulus

The measure of the resistance of one material to volumetric compression is known as bulk modulus. The modulus is defined as the ratio of hydrostatic stress (σ) relative to the volumetric stain (ε), which is determined from the stress-volumetric strain curve.[13]

$$K = \frac{\sigma}{\varepsilon} \qquad (1.4)$$

The volumetric strain data are presented by plotting the strain percentage (x-axis) against the axial stress [MPa] as the y-axis. There are different methodologies to determine the bulk modulus, including secant modulus between the origin and any point (a), tangent modulus at any stress (b), chord modulus between two points (c), and initial trend modulus (d) as shown in Figure 1.2. Each modulus results in different output, dependent on the shape of the loading curve.

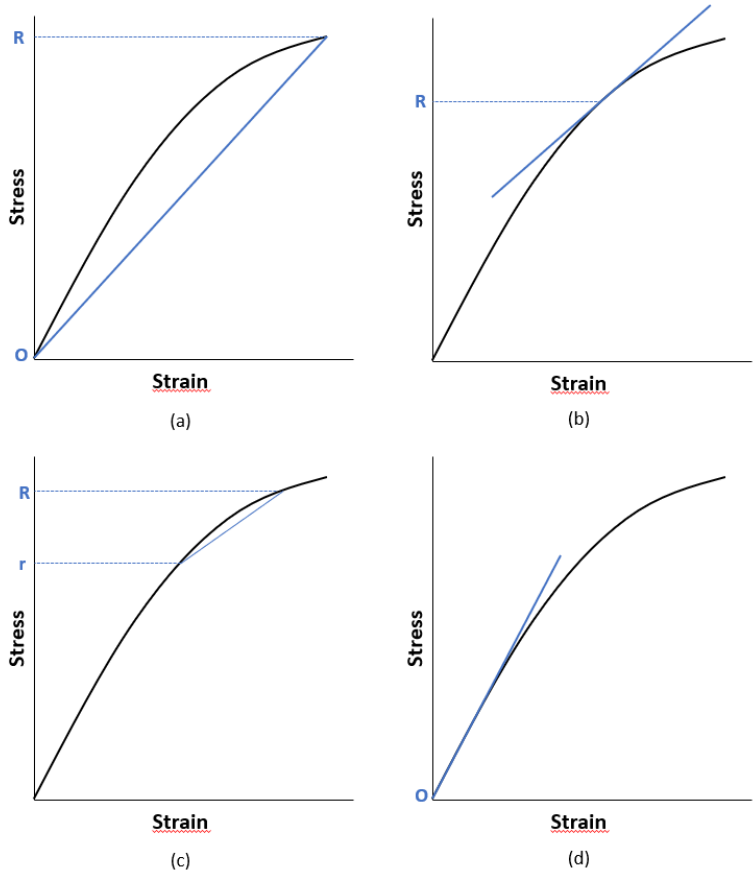

Figure 1.2 - Bulk modulus determination method

In this study, the secant, trend line, and chord modulus were used to determine the bulk modulus. The secant modulus is the slope of a line drawn from the origin of the stress-strain diagram to an intersecting point of interest. Therefore different bulk modulus values can be collected depending on the point of intersection. The chord modulus is the slope of a line drawn between two specified points on the stress-strain curve. To maintain a comparable dataset, the bulk modulus in this study is calculated between the two confining pressure intervals of origin - 3 MPa (secant modulus), origin – maximum stress (trend line), and 5 MPa - 7.5 MPa (chord modulus). These intervals are suitable for all three confining test pressures. Figures 1.3 and 1.4 present how three different methodologies can affect the output of bulk modulus calculation depending on the test result and its trend.

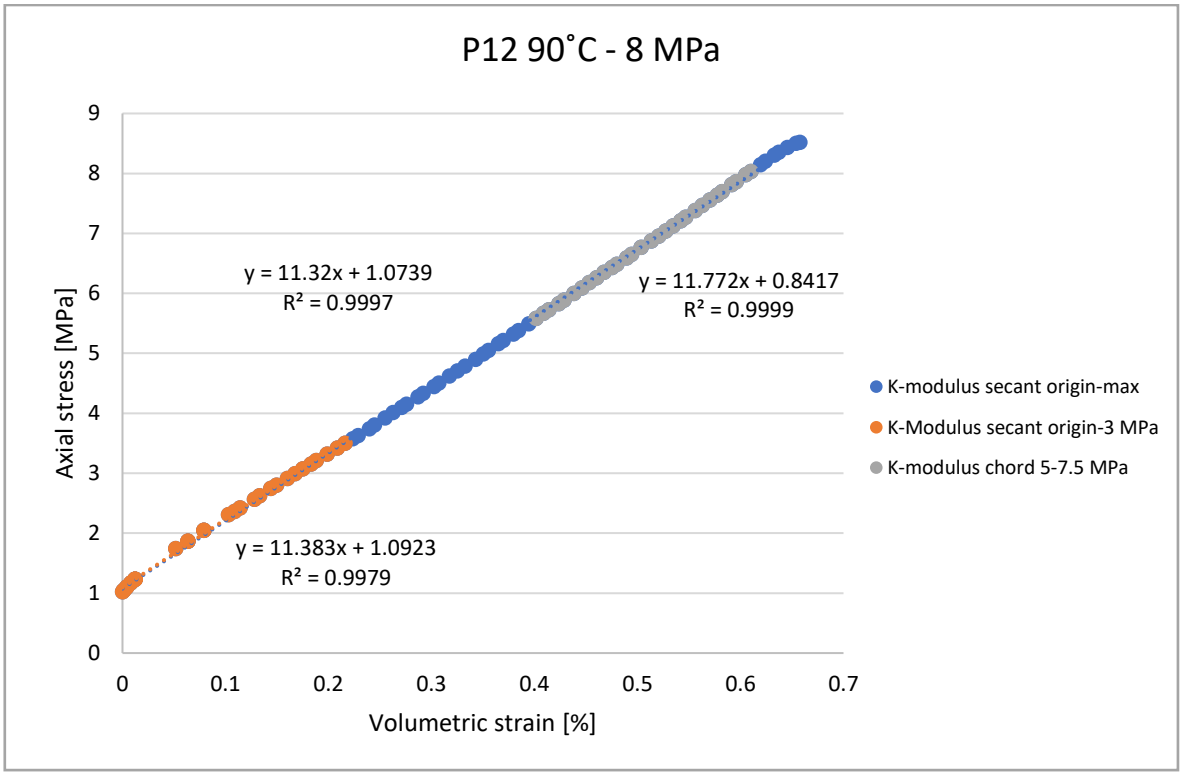

Figure 1.3 - P12 minor K-modulus variation

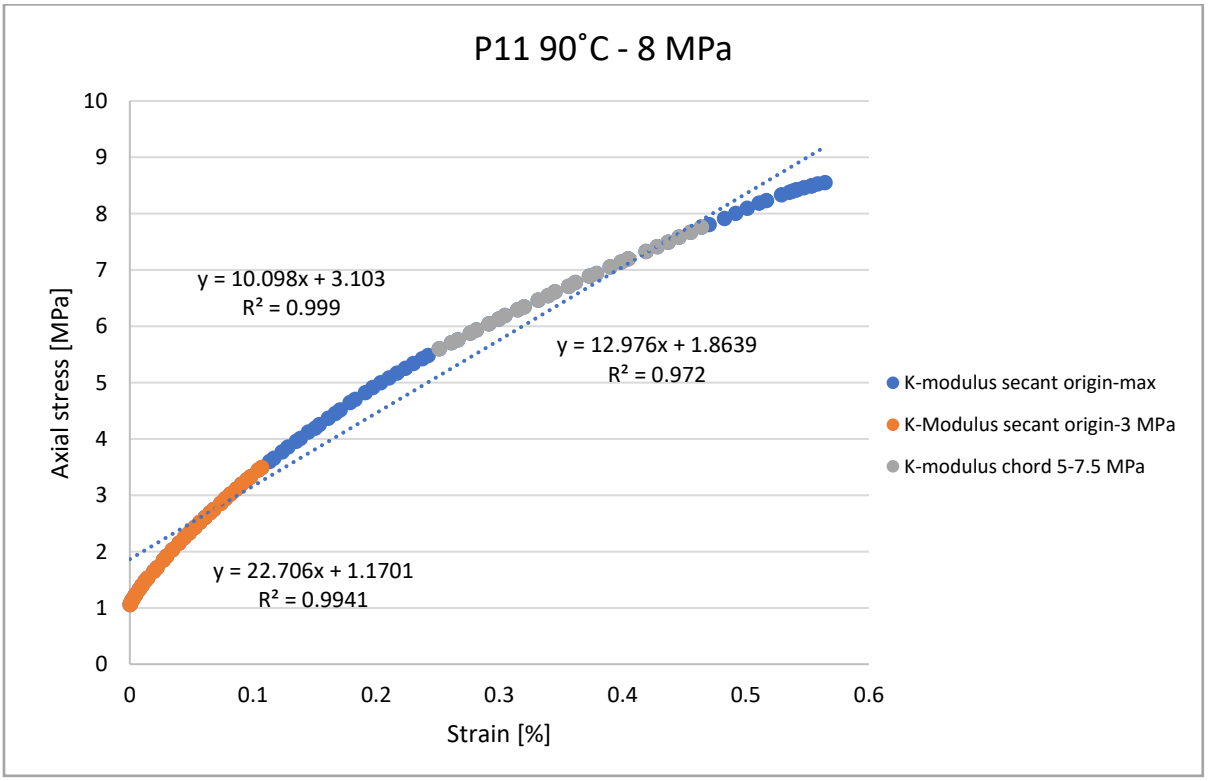

Figure 1.4 - P11 major K-modulus variation

The data presented in Figure 1.3 is taken from the test result of P12 at 8 MPa confining pressure, where the plotted data is an approximate linear growth. In this scenario, the bulk modulus will not significantly vary with the use of different methods determining bulk modules. On the other hand, the plotted data in Figure 1.4, which belongs to test P11 at 8 MPa confining pressure, demonstrates how three different methods can generate various bulk modulus outputs.

1.3.5 Young's Modulus

A measure of the stiffness of a solid material is known as elastic or Young's modulus. The modulus is defined as the ratio of axial stress (σ) applied to a solid material relative to axial strain (ε) produced within the elastic limit of the material itself, as shown in Eq. 1.5. Beyond the elastic limit, the material will deform, and it will not return to its original dimension after the stress is removed. Simply, it determines the amount a material deforms under a given load. Young's modulus was introduced first in 1807, and since then, it has been an important measurement to measure the stiffness of a material. High Young's modulus indicates low flexibility and is more desirable for applications requiring high stiffness, such as construction applications. Materials with low Young's modulus are desirable for applications with flexibility.

$$E = \frac{\sigma}{\varepsilon} = \frac{Stress}{Strain} \qquad (1.5)$$

In this study, Young's modulus is determined using axial strain data collected during deviatoric loading. The secant modulus method is used to determine the coefficient of the initial trend, as presented in Figure 1.5. Young's modulus parameters have been calculated in the piston pressure interval of the origin to 5 MPa to achieve comparable data.

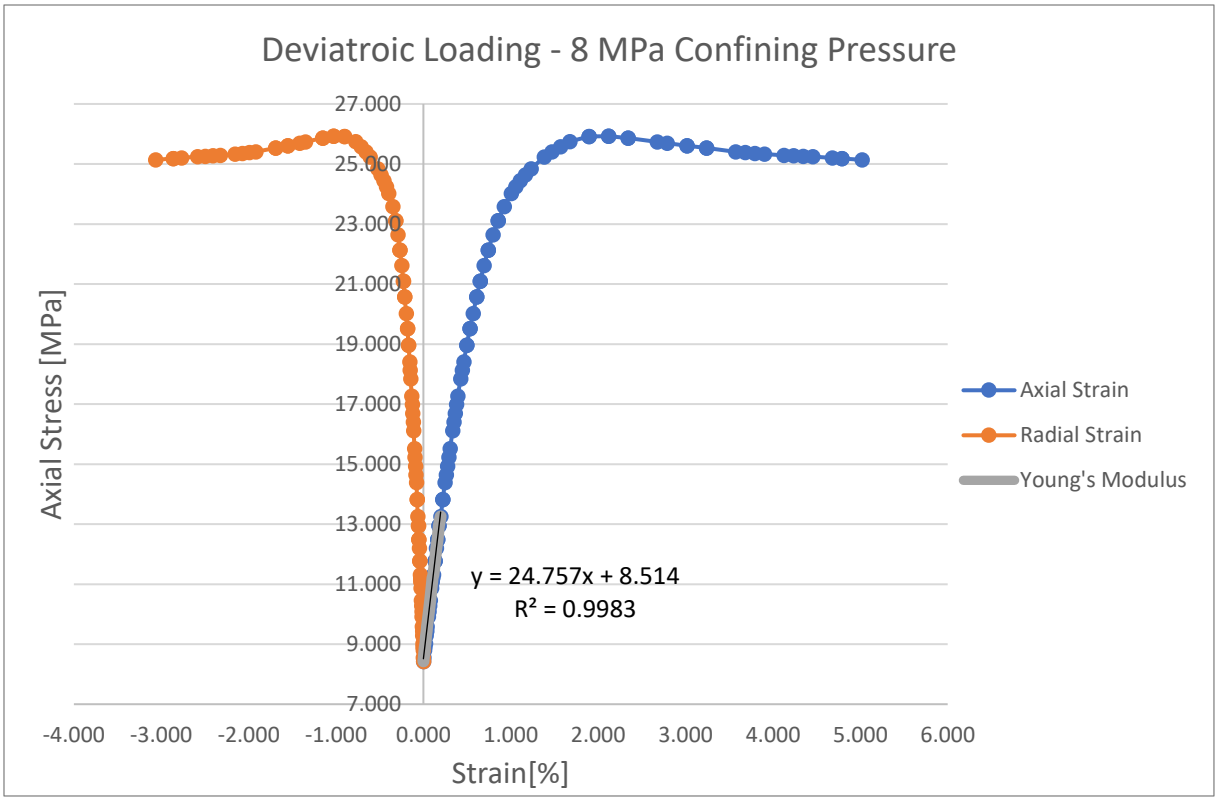

Figure 1.5 - Young's modulus determination

1.3.6 Poisson's Ratio

The ratio of the axial strain to the radial strain is known as Poisson's ratio. It is a measure of the deformation of the specimen in a direction perpendicular to the direction of compression. The Poisson's ratio for most materials is positive since they tend to get thinner in cross-section when stretched. Poisson's ratio is an important material property among cement-based materials since lateral deformation results in causing cracks and can have significant implications for their structural integrity over time. Therefore having a lower Poisson ratio can improve the resistance of cementitious material to shrinkage and cracking. In this study, the linear regression analyses for both Young's modulus and Poisson's ratio are obtained from the same axial stress interval.

$$\nu = -\frac{\varepsilon}{\varepsilon} = \frac{Lateral\ Strain}{Longitudinal\ Strain} \qquad (1.6)$$

1.3.8 Failure Mechanics

A failure will occur when a core is subjected to sufficiently large stresses, is permanently changed in shape, and has the potential of falling apart. Following a failure, the core will have a reduced ability to carry loads. Having an understanding of petroleum-related rock mechanics is important to predict conditions a core will reach to its failure to prevent instability and well integrity problems. The strength of a core is defined as the stress level at which the core fails. However, the phrase stress level is a parameter that is not defined uniquely, making strength also a unique parameter. Therefore, strength is only a meaningful parameter when the test is done in a specified laboratory setting. The most important methods used to measure core strength are triaxial and uniaxial tests which give great definitions of the complexity of core failure. A typical test specimen (core) is a cylinder with length to diameter ratio of 2:1, just as illustrated in Figure 1.6. The suggested core diameter for petroleum applications is 38.1 mm (about 1.5 in).

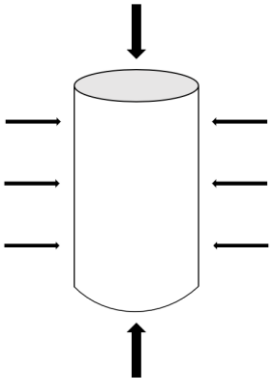

Figure 1.6 - Typical test core for uniaxial and triaxial tests

The axial stress is applied to the end faces of the cylindrical core by a pair of pistons. If no confining stress is in place, a uniaxial stress test is performed. On the other hand, if the confining pressure is non-zero, the test is known as a triaxial test. A triaxial test is performed by increasing confining and axial loads simultaneously until reaching a prescribed hydrostatic stress level. Afterward, the confining pressure remains constant while increasing the axial load until core failure is reached. The stresses causing failure are known as the effective stresses that are felt by the framework. Effective stress is defined as the confining pressure or axial stress subtracted by the pore pressure. In triaxial and uniaxial compression tests, shear failure is the most common type and occurs when excessive shear stress is applied. Pore collapse is another failure mode caused by excessive hydrostatic stress or high confining pressures, but it is most

common to occur on samples with high porosity. Relevant types of failure modes that the core can experience are defined in the following subchapters.

1.3.8.1 Shear Failure

When the shear stress along some plane in the core is sufficiently high, shear failure occurs. As a result, a fault zone will develop along the failure plane, and both sides of the plane will move in a frictional process relative to each other, as shown in Figure 1.7. The force that presses the two planes together defines the frictional force between the two bodies of the core. Therefore, it is assumed, based on Mohr's hypothesis, that the critical shear stress, which is the reason for shear failure, is dependent on the normal stresses acting on the failure plane.

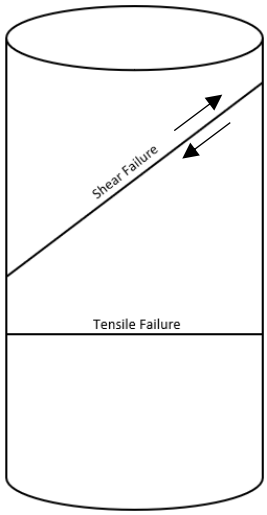

Figure 1.7 - Shear failure vs tensile failure

1.3.8.2 Compaction Failure

Compaction failure or pore collapse is when core grains may break or loosen and then be twisted or pushed into the available free pore space, resulting in closer and greater packing of the material as illustrated in Figure 1.8. This type of failure typically occurs in material with high porosity, where the grains are structured relatively open. As mentioned previously, pore collapse can occur due to pure hydrostatic loading. However, by microscopically analyzing this failure mode, its main reason for failure is excessive shear forces acting through the grains. Hence, the source of pore collapse and compaction failure is a shear failure within the material of the core. Another source of compaction failure that may occur under hydrostatic loading is grain crushing which results in the splitting crushing of the grains due to sufficiently high stresses. Both failure mechanisms lead to permanent damage to the core framework and cause a reduction in stiffness and yielding of the core. It is important to note that compaction failure

or pore collapse can also occur under non-hydrostatic stress conditions. Therefore, it is common to observe this type of failure in triaxial tests with high confining pressure.

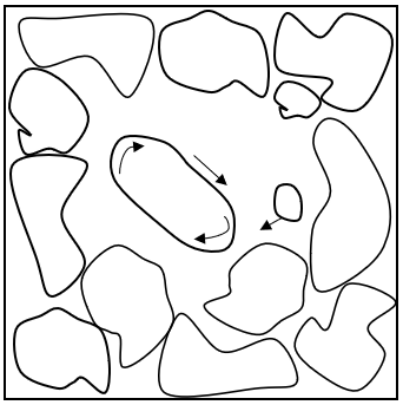

Figure 1.8 - Reorientation of grains resulting in a close packing

1.3.8.3 Mohr's Circle

In the field of rock mechanics, having an understanding of stress and strain conditions is crucial for analyzing the behavior of structures and materials. Mohr's circle is a great graphical tool that briefly explains stress states at a point and facilitates the determination of stress transformation, maximum shear stress, and principal stresses. To present Mohr's circle, stress states at different orientations are plotted and transformed using the stress transformation equations. The y-axis represents shear stress, and the x-axis represents normal stress. The average normal stress corresponds to the circle's center, and the radius represents the maximum shear stress. The diameter's endpoints passing through the center are where the principal stresses are located.

1.3.9 Mechanical Properties Measurement

The only way to measure in situ rock mechanical behavior is through rock mechanical core analysis. This allows the measuring of static elastic and strength parameters. The analysis must be designed according to the purpose of the study and investigation. For instance, if the objective is to analyze borehole stability, the tests and testing procedure will not be the same as the investigation of reservoir compaction. Another factor that must be considered during mechanical properties behavior testing is the type of rock or material that will be tested. Some rock types, such as shales, need special test and preparation procedures. There are numerous methods to determine in-situ stresses; however, for this study, a triaxial test is the most relevant test method to use. To achieve reliable determination of static elastic and strength parameters, it is crucial to have the proper equipment, test, and preparation procedures.

1.3.9.1 Core

The core is the source of the measurement during a rock mechanical analysis. Hence, comparative studies must have a consistent and representative sample throughout the whole research. As the samples tested in this study are made in the laboratory, consistent raw material and preparation procedures are key.

1.3.9.2 Laboratory Equipment – Triaxial Test Cell

The triaxial cell is the second most important element in the test system. There are two types of triaxial cells being used in analyzing rock mechanics. The Hoek triaxial cell where the sample is placed in between two movable pistons. The other system, which is used in this study, uses a fixed pedestal carrying the sample on the bottom, and a movable loading piston on the top. A standard rock mechanical test laboratory equipment consists of the following segments:

- Triaxial cell.
- Axial and radial measurements equipment (LVDT and extensometer)
- Confining pressure system.
- Pore pressure system.
- Pump to provide the needed pressure.
- A computer used for data processing and control.

A triaxial cell consists of a cylindrical specimen chamber, typically made of acrylic or stainless steel. The triaxial cell chamber is divided into two separate chambers: the confining chamber and piston chamber. The piston chamber applies axial stress to the top of the core, while the confining cell applies uniform pressure to the sample. The pore pressure is controlled by the use of a back pressure regulator. The triaxial cell design and test setup have a major impact on the collected data; therefore, some design requirements are followed to minimize error and achieve repeatable data.

It is crucial to have a well-designed contact surface between the equipment and the core to achieve reliable data. Therefore both sides of the core sample must get evened before testing. A shrinkage sleeve is placed around the sample to avoid contamination and separate the sample from the confining fluid. It is also important to use a soft enough sleeve to prevent providing significant support to the sample. The specific triaxial cell used in this study is presented and described in Chapter 3.2.7.

1.4 Previous Studies

To familiarize the process of well integrity management and design, a global approach to designing cement sheath integrity is taken. Companies require cement specifications which is beneficial for both service and operator companies. Compressive strength is currently the standard to characterize the mechanical properties of the cement, which is not satisfactory and sufficient. Parameters such as elastic properties, tensile strength, and failure criterion must be included since they describe the cement's true compressive strength. To collect mentioned properties, tests developed by available rock mechanics, such as triaxial testing, can be used. A standard testing procedure must be implemented to have a common language and clear communication between companies.[14] Many parameters during triaxial testing can affect the mechanical properties collected, such as confining pressure and test temperature.

During studies done by Meng et al. (2022) on in-situ mechanical properties of OPC, the confining pressure was varied between 10, 20, and 40 MPa through cyclic compression. The result was an increase in Poisson's ratio and elastic modulus with confining pressure.[15] However, other researchers such as Zheng and Lima (Zheng et al. 2017; Lima et al. 2022) observed otherwise. During their study, the cement paste got more ductile following confining pressure increase, and Young's modulus was reduced.[16, 17] Li et al. (2019), on the other hand, did not observe a significant effect of confining pressure on the elastic modulus of OPC.[18] Based on the study done by Jimenez et al. (2019), the mentioned inconsistency in the effect of confining pressure was studied. As a result, the study concluded that the curing conditions mainly caused the discrepancy. Jimenez and Meng had the same curing pressure as the testing pressure during their studies and experienced an increase in elastic modulus and Poisson's ratio with confining pressure increase. On the other, Zheng and Lima did not have consistency in the curing and testing conditions, resulting in a decrease in elastic modulus and Poisson's ratio with an increase in confining pressure.[19] This shows the importance of sample preparation and testing procedure and why a standard preparation and test procedure must be implemented in the industry.

Adijat Ogienagbon et al. (2022) studied the effect of temperature on the mechanical properties of different setting materials, including two-part granite-based geopolymer, class G cement, expansive cement, and thermosetting resin.[20] The parameters analyzed in the study were determined with the same methodology as this project. Geopolymer had the lowest Young's modulus among these setting materials at a test temperature of 30°C (4 GPa), and it retained its flexibility when the test temperature was increased to 90°C (3.5 GPa). A large strain-

bearing capacity was also observed in the geopolymer samples during axial compression, which was also mentioned in a study by Kimanzi et al. (2020).[21] Materials with low Young's modulus are less likely to reach failure and, therefore, can maintain zonal isolation at elevated and low temperatures.

An increase in test temperature increased Poisson's ratio in all the selected materials, and geopolymer and thermosetting resin were the samples most sensitive to temperature. The Poisson ratio of the geopolymer increased from 0.19 to 0.30 with the increase of test temperature from 30°C to 90°C. An increase in Passion's ratio will decrease the shear stresses included in the material and the magnitude of the destructive hoop, reducing the risk of failure (Kwatia et al. 2017).[22] An increase of Poisson's ratio of the material at elevated temperature means higher flexibility and ability to withstand deformation in bottom hole conditions, leading to great long-term integrity (Therond et al. 2017).[23]

Since the triaxial cell was also used in Adijat's study, the confined compressive strength of the material was also analyzed, and the sensitivity of this parameter to temperature was confirmed. Despite the constant curing temperature, the increase in test temperature caused the reduction of the confined compressive strength or yield strength. The average compressive strength of the geopolymer samples reduced from 55 to 38 MPa, while the strength of neat class G cement reduced from 72 to 67 MPa. However, this does not mean geopolymer is weaker than class G cement at elevated temperatures.

Studies have shown that the compressive strength to Young's modulus ratio is more important than their individual parameters to zonal isolation (Kamali et al. 2021; Jafariesfad et al. 2017).[6, 24] A preferable zonal isolation material should have a low Young's modulus and high compressive strength. (Jafariesfad et al. 2017). Therefore, despite the low compressive strength of the geopolymer samples, it has a higher ability to maintain zonal isolation than the other studied materials due to its low Young's modulus.

At last, the effect of confining pressure was analyzed by Adijat, and a major difference in the compressive strength was observed between the confined and unconfined tests. Geopolymer experienced and 300% increase in compressive strength because of confining pressure, while class G cement had an 82% increase. Therefore, it got concluded that the increase in confining pressure increases the compressive strength of the zonal isolation material.

2 Objective

Geopolymer is one of the materials extensively being explored for utilization in the petroleum and construction industries and has garnered significant interest. In order to characterize the rock mechanical properties of geopolymers, triaxial testing has been conducted, following the industrial standards developed for characterizing the rock mechanical properties of OPC (Ordinary Portland Cement). However, a crucial question arises regarding the applicability of these standards to geopolymers, particularly those based on granite, or if new industrial standards need to be developed.

To address this question, a sensitivity analysis is required to determine the parameters necessary for studying the rock mechanical properties of geopolymers. This study focuses on investigating the sensitivity of geopolymers to temperature and confining pressure. The experiments are done with the use of a triaxial cell with the test matrix presented in Table 2.1.

Table 2.1 - Test Matrix

Test Temperature	Confining Pressure
30˚C	8 MPa, 17.2 MPa, 26 MPa
60˚C	
90˚C	

3 Materials & Analytical Methods

In-situ mechanical properties of a GPC can be varied with different materials and chemicals used to prepare the mixture. There are in addition, different methodologies on how mechanical properties of a cementitious material are analyzed. This chapter presents the chemical, materials, equipment, and procedures used in this study.

3.1 Materials

Geopolymer cement is composed of precursors and an alkaline activator (hardener). The precursor is from a source material rich in silica and aluminum. This study used granite from the mining industry to produce a rock-based geopolymer. Commercial aluminosilicate minerals were added to normalize the chemical composition of the used rock. Since one-part geopolymer cement has been investigated in this study, the activator is added to the precursor as powder. Each component is briefly described in the following two chapters.

3.1.1 Precursor

The raw material used in the rock-based geopolymer mixture is based on waste material from the granite mining industry. The precursor weighs 700 grams consisting of a mixture of raw material, micro-silica, and GGBFS. The solid phase hardener is later added to the precursor.

3.1.2 Alkali Activator - Hardener

The activator, also known as the hardener, can be added in both liquid and solid phases. In this study, solid-phase potassium silicate is added to the precursor as an alkali activator. A small amount of 12 molar potassium hydroxide is used as an accelerator. In further studies done by the research team at UiS, a one-part GPC recipe is generated without adding KOH as an accelerator. This type of geopolymer recipe is called “just add water GPC” which are more friendly for offshore usage compared to the conventual two-part geopolymer recipe.

3.2 Equipment

Several pieces of equipment besides the triaxial cell are used in this study. Each piece of equipment is described with respect to the order of usage in a test run.

3.2.1 Mettler Toledo Scale

For measuring the weight of the components used to create a geopolymer slurry, a Mettler Toledo scale with an accuracy of +/-0.01g is used. To minimize error, only one scale is used for this study, presented in Figure 3.1.

Figure 3.1 - Mettler Toledo scale

3.2.2 OFITE Model Commercial Blender

OFITE commercial blender is used in this study to prepare the slurry and mix the precursor with the liquid phase. The blender follows API procedure standards and is equipped with a pre-programmed blending setting used to mix the geopolymer slurry. The pre-programmed setting mixing duration lasts 50 seconds and consists of two phases. The first phase lasts 15 seconds, where the blending speed is 4000 RPM. The intention of having low RPM in the beginning is to add the precursor to the liquid phase with minimized dust, losses, and spillage. The rest 35 seconds of the blending time is programmed to have a blending speed of 12000 RPM to ensure a homogenous mixture. The commercial blender used in this study is presented in Figure 3.2.

Figure 3.2 - OFITE commercial blender

3.2.3 Atmospheric Consistometer

After mixing the geopolymer cement, the slurry is poured into a container with a blade in the middle. The container is afterward placed in the atmospheric consistometer. The atmospheric consistometer (ATM consistometer) simulates bottom hole circulation at atmospheric pressure with a temperature ramp up and it follows API standards spec 10A/10B2. A consistometer is commonly used to measure consistency (workability and setting time) or to condition the slurry. In this study, this equipment is used for conditioning the geopolymer slurry before curing it in high-pressure and temperature conditions. The ATM consistometer used in this study is presented in Figure 3.3.

Figure 3.3 - Consistometer (left) and container setup (right)

3.2.4 Molds

The conditioned slurry is poured into curing molds specially designed for triaxial testing for petroleum applications. The mold is made of steel and has a plastic top lid, as shown in Figure 3.4. The top plastic lid has a small hole allowing communication between the sample and the environment in the autoclave, which is in high pressure and temperature condition. The inside of the molds is covered with silicon grease from Biltema to avoid bonding and reduce sample removal difficulties. The silicon grease is replaced midway through the study with high-temperature and high-pressure red grease commonly used in the oil and gas industry.

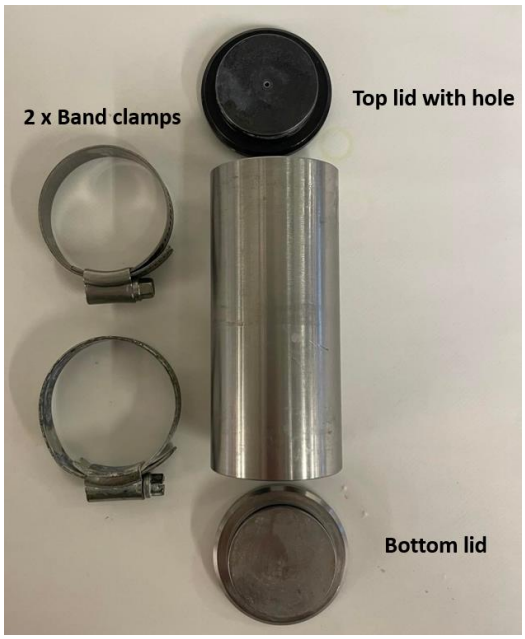

Figure 3.4 - Curing molds

3.2.5 Autoclave & Oven

The filled-up molds are placed into the autoclave, illustrated in Figure 3.5. Prior to that, the autoclave is filled with water with a matching temperature to the conditioning temperature. This is to prevent the samples from suffering from temperature shock. The autoclave is then placed in an oven where it is connected to a pump to enable the increase of pressure.

Figure 3.5 - Autoclave (left) and curing oven (right)

3.2.6 Cutting & Grinding Machine

A small hole is made on the top lid of the molds to enable the pressure connection between the autoclave and the mold. This design also leads to contamination of the core's top part, which can give unreliable data. Therefore, it is important to cut the contaminated part of the core while maintaining the desired length to be able to run the test. The cutting is done using the cutting machine presented on the left of Figure 3.6. To achieve reliable mechanical properties data, it is crucial to have even surfaces so the force is distributed evenly along the whole surface of the core during the triaxial test. Therefore, the core's top and bottom are evened with the use of a grinding machine presented on the right of Figure 3.6.

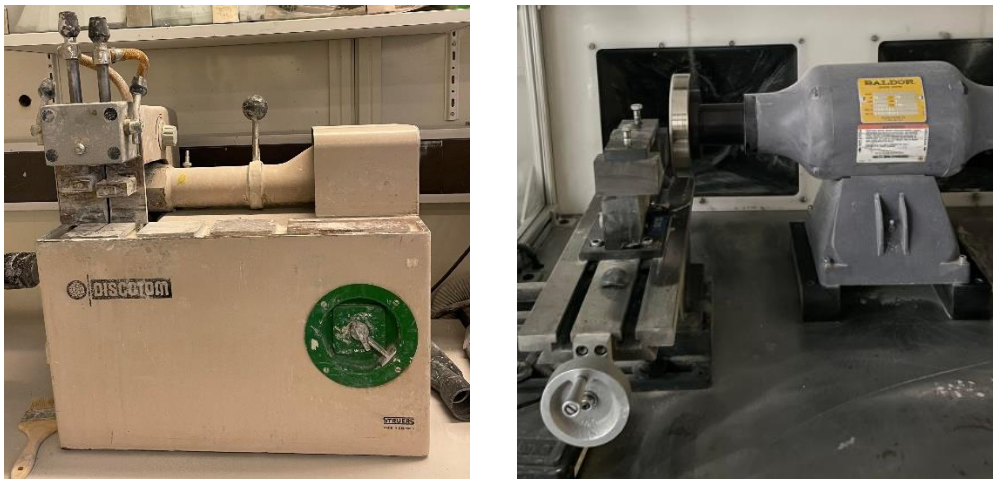

Figure 3.6 - Cutting machine (left) and grinding machine (right)

3.2.7 Triaxial Cell

As described in chapter 1.4.4, the triaxial cell is used to replicate the in-situ stresses of geopolymer cement in the wellbore and determine its mechanical properties. The specific triaxial cell used in this research is presented in Figure 3.7. An internal illustration of the test setup is also presented below in Figure 3.8, giving a great overview of how the setup operates. The LVDT at the top of the setup and the extensometer around the core is responsible for monitoring length and diameter changes, respectively. During a test, the confining pressure is firstly increased by injecting mineral oil through confining inlet, into the confining chamber. After reaching the required confining pressure, the piston is moved down to the top of the core by pressurizing the piston's upper chamber through the piston pressure inlet. The axial pressure is increased until either LVDT or extensometer reaches out of range, and no data is longer collected. The outlet line of each chamber is used to depressurize the test setup prior to disassembling the cell. All the tests run in this study are without pore pressure; therefore, the pore pressure control valve has been kept close throughout the study. Data collected from the

pressure meter, LVDT, and extensometer are used to calculate Young's modulus, bulk modulus, Poisson's ratio, and yield strength.

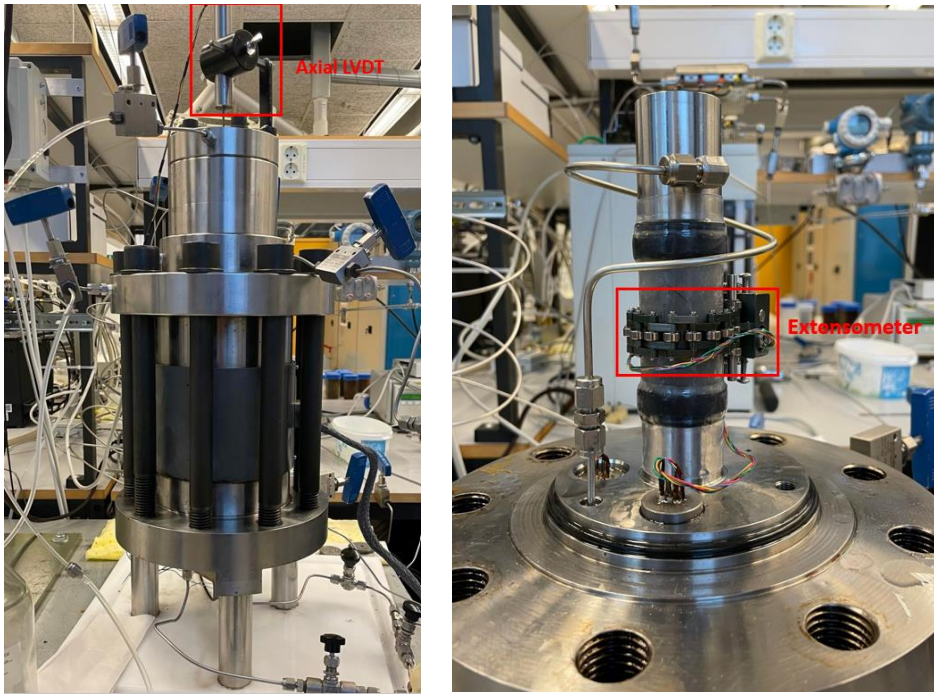

Figure 3.7 - Triaxial cell used in this study

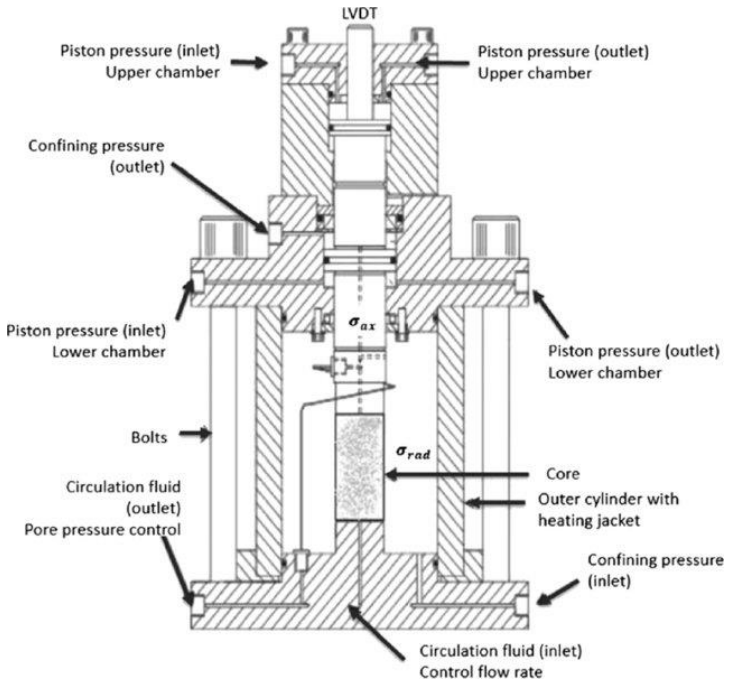

Figure 3.8 - Internal illustration of the triaxial cell [25]

3.2.8 Pump

Pumps have been highly implemented in this study since the in-situ properties of the material are analyzed under high pressure. There has been used two types of pumps in this study. Figure 3.9 presents the VP-12K-SS pump by Vindum Engineering, which has been used to pressurize the autoclave up to 2000 psi and keep the pressure constant during one week of curing. The figure on the right presents the QuizeX pump by Chandler Engineering, which has been used to pressurize and depressurize the piston and confining chamber of the triaxial cell.

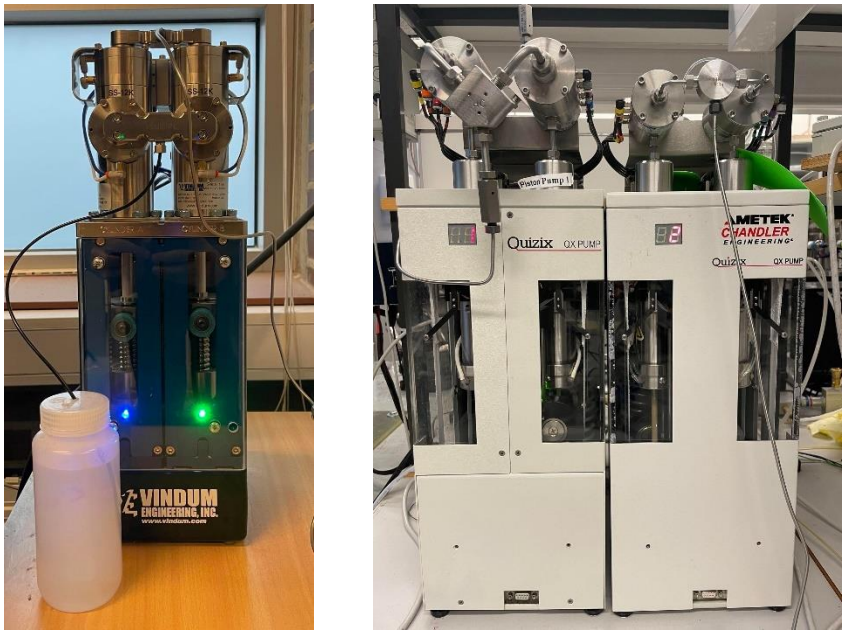

Figure 3.9 - VP-12K-SS pump (left) and QuizeX pump (right)

3.3 Procedures

The procedures involved in this study are presented in order in the following sub-chapters.

3.3.1 Mixing

There are different ways of preparing geopolymer slurry; however, to achieve reliable data, it is crucial to have a consistent mixing procedure for all the samples. The following mixing procedure is followed throughout the entire project:

1. Weight components of the precursor with the use of the Mettler Toledo scale.
2. Mix the precursor in a dry condition (bucket with a lid).
3. Weight required water and KOH.
4. Mix the two phases as described in Chapter 3.1 with the use of OFITE Model Commercial Blender.

5. Use a spatula to minimize the losses by leading all the precursors into the mixture during mixing.

3.3.2 Conditioning

The conditioning is done according to API Spec 10A/10B2 standards, and it has been followed through as below.

1. Prepare the ATM consistometer cell with its blade paddle placed correctly in the middle of the cell.
2. Fill the cell with slurry up to the marked maximum limit.
3. Mount the lid shown in Figure 3.3. Important to make sure that the paddle is connected to the torque shaft.
4. Place the cell into the consistometer.
5. Switch on the main and heat button and set the temperature to 30°C.
6. Condition the slurry for 30 minutes after it has reached 30°C. It takes approximately 10 minutes to increase the temperature from ambient to 30°C.

3.3.3 Curing

After conditioning the slurry, the following steps are taken to cure the samples:

1. Prepare the metallic molds by greasing the container and both lids.
2. Fill the autoclave with approximately 30°C water while the slurry is conditioning.
3. Pour the conditioned slurry into the molds. Make sure there is no leakage.
4. Place the molds into the autoclave and close it.
5. Place the cell in the 90°C oven and pressurize the cell up to 2000 psi using the VP-12K-SS pump.

3.3.4 Triaxial Testing

After one week of curing, the autoclave is removed from the oven and is set to cool down and depressurize. The cores are then taken out, and the following procedure is applied to complete the triaxial test:

1. Cut the top of the core where most contamination has occurred (75 millimeters or less).
2. Even out both sides of the core using the grinding machine.
3. Prepare shrinkage sleeve and filter paper.
4. Place rubber band, drainage plate, and filter paper on top and bottom of the core as shown below in Figure 3.10.

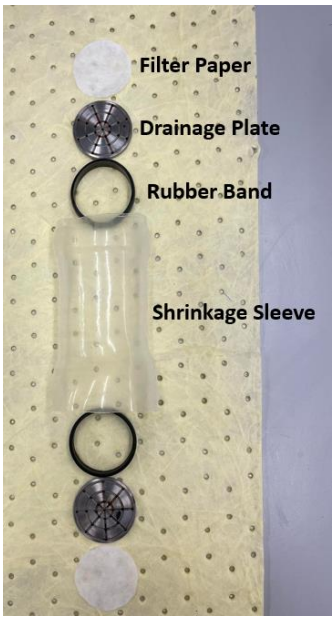

Figure 3.10 - Core preparation setup

5. Place the core on the triaxial setup.
6. Put on the extensometer and the top lid.
7. Use a heating gun to secure the sample in place and protect it from contamination. The final result is presented on the right side of Figure 3.7
8. Install confining chamber and fill the chamber with oil.
9. Install the top part by tightening the bolt using a torque wrench with a preset torque.
10. Install axial LVDT on top of the top part.
11. Increase the confining pressure to 0.5 MPa and move the piston down, on top of the core. It is important to stop the piston immodestly after contacting the core to minimize fatiguing the core prior to the test.
12. Turn on the heater to the desired temperature.
13. Run the test the day after by first increasing the confining pressure and then increasing the piston pressure till failure of the core.
14. Wait for the cell to cool down and disassemble.

4 Result & Discussion

During this study, 18 geopolymer cement plug samples with the same recipe were tested, and the test matrix is shown in Table 4.1. Two tests were run on three different temperature variations (30°C, 60°C, 90°C) at three different confining pressure of 8 MPa, 17.2 MPa, and 26 MPa. The following chapter presents and discusses the effect of temperature and confining on the axial, radial, and volumetric strain during hydrostatic and deviatoric loading. Additional parameters such as Young's modulus, bulk modulus, and Poisson's ratio are also mentioned for better understanding and comparison. To simplify the data reading, all the temperatures have a specific color and are as follows: 30°C as blue, 60°C as yellow, and 90°C as orange. Since two tests are run per temperature, the first test is presented as a full line, and the second test is presented with a dotted line for easier reading.

Tabell 4.1 - Test matrix

Sample	Temperature [°C]	Confining Pressure [Mpa]	Length [mm]	Diameter [mm]
P1	90	17.2	74.45	37.89
P2	90	17.2	69.98	37.94
P3	30	17.2	75.42	37.95
P4	30	17.2	68.55	37.99
P5	60	17.2	62.25	37.87
P6	60	17.2	74.14	37.94
P7	60	8	72.61	37.94
P8	60	8	75.52	37.93
P9 (19)	30	8	73.89	37.96
P10	30	8	72.11	37.98
P11	90	8	71.64	38.01
P12	90	8	71.96	37.95
P13	90	26	73.5	37.96
P14	90	26	75.48	37.96
P15	30	26	74.11	37.97
P16	30	26	72.66	38.02
P17	60	26	73.16	37.97
P18	60	26	74.13	38.07

Throughout the study, a high degree of unrepeatability was observed during the first seven tests. To prevent such inconsistency in the results, the sample preparation procedure was analyzed to detect potential errors and slurry contaminations. Furthermore, changes were applied in the methodology of the sample preparation. These changes were crucial for the study, and the information is needed for analyzing the results.

As mentioned in Chapter 3.3.4, the inside of the curing molds is covered with silicon grease from BiltemaAS to avoid sample removal difficulties. The consistency of this grease was too low, leading to potential contamination of the slurry. In addition, the samples got highly damaged during removal from molds due to their strong bonding to the mold's surface. Hence, following the sixth iteration (P6), the grease was changed to Superfilm UCA grease. After this change, no damage was done to the core sample during sample removal.

After the mixing procedure is done, the slurry is conditioned for 40 minutes. When pouring the slurry into the curing molds, it was observed that it had low viscosity at first (mold #1) and high viscosity at the end (mold #4). In other words, the slurry was not homogeneous. Hence, from test P7, the slurry was slowly stirred after conditioning to avoid the settlement of particles and a non-homogeneous slurry. In addition, the molds were marked in order, representing their order in the autoclave and order of filling, as presented in Figure 4.1.

After filling up the molds, a small amount of water was added on top of the slurry to speed up the pressurizing of the molds inside the autoclave. When the top lid of the mold (Figure 3.4) was installed, part of the additional water got removed through the small hole on the top lid. However, the water was not clear, and it was partially mixed with the slurry. Therefore, the placed water was removed from test P8 to avoid contamination of the slurry.

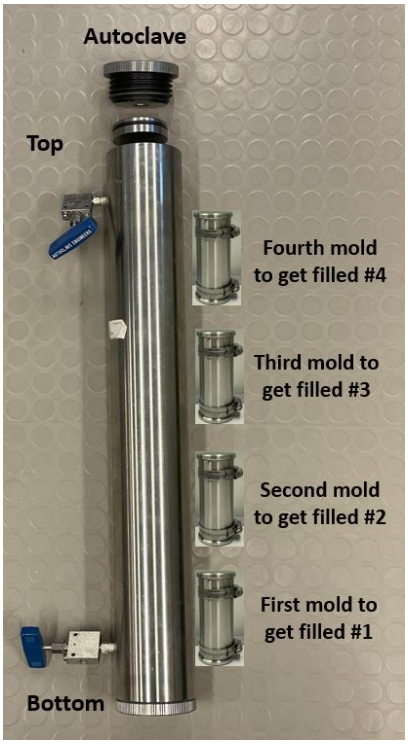

Figure 4.1 – Order of mold placement

4.1 Result

This chapter presents the result of hydrostatic and deviatoric loading at three confining pressures of 17.2, 8, and 26 MPa.

4.1.1 Confining Pressure 17.2MPa

4.1.1.1 Hydrostatic loading

As presented in Figure 4.2, the geopolymer samples have poor repeatability in the hydrostatic loading phase. P5 and P6 should have corresponding results at 60°C; however, it is visible that the axial strain difference is significant. P5 has an axial strain of 0.56%, whereas its corresponding test has an axial strain of 1.42%. The same repeatability issue is observed in samples tested at 90°C and 30°C tests; therefore, it is not possible to conclude the effect of test temperature on the axial strain at 17.2 MPa.

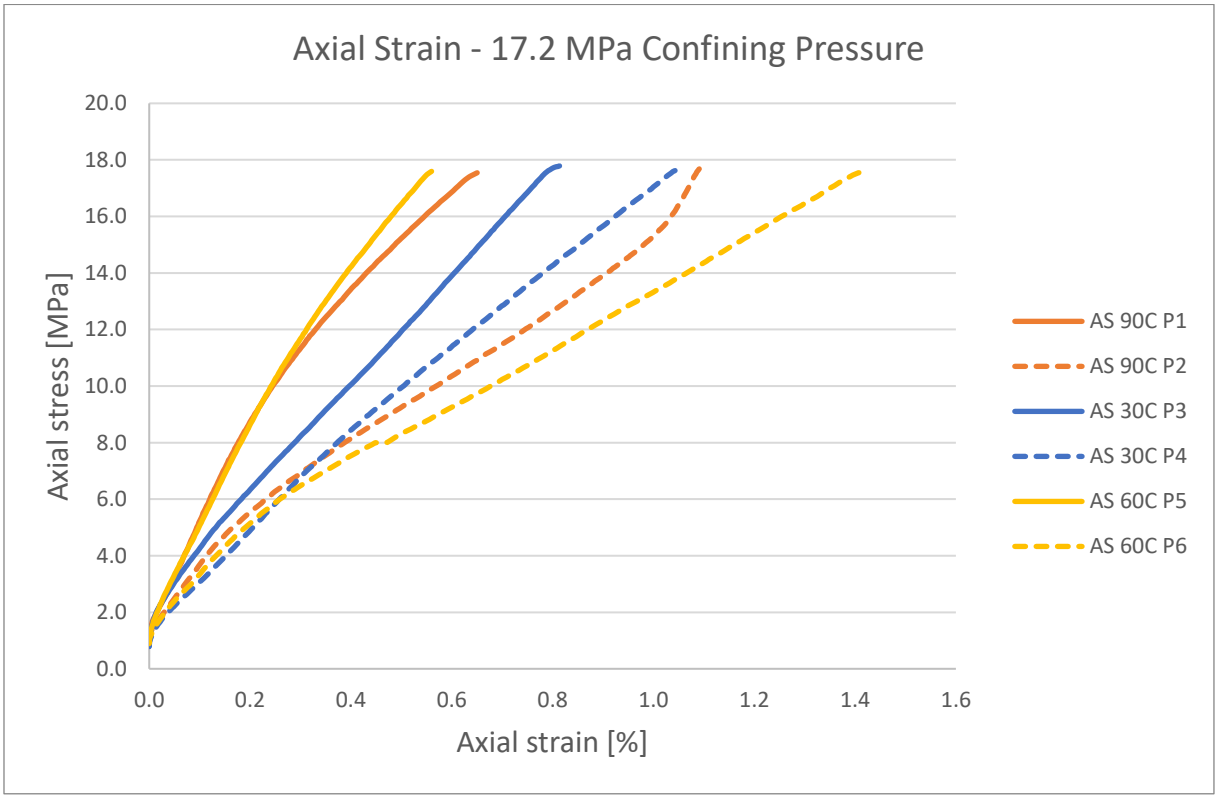

Figure 4.2 - 17.2 MPa confining pressure axial strain hydrostatic loading

The poor repeatability of the core sample is also visible in the radial strain, just as in the axial strain. The difference in radial strain is significant between the corresponding test at 30°C (P3&P4) and 90°C (P1&P2), as shown in Figure 4.3.

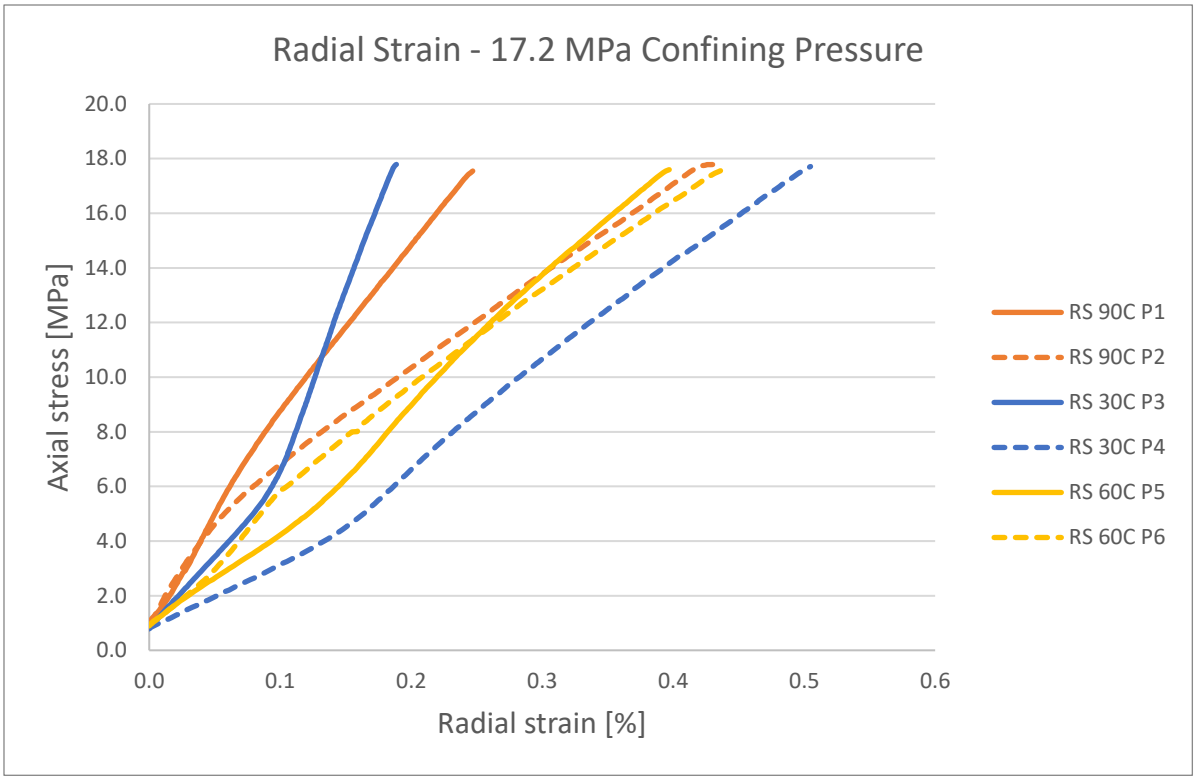

Figure 4.3 - 17.2 MPa confining pressure radial strain hydrostatic loading

Similar to previous data collected at 17.2 MPa confining pressure, poor repeatability is visible on the volumetric strain, as presented in Figure 4.4. The corresponding tests are not representative, and it is a confirmation of inconsistency or potential error in either sample preparation or raw material used.

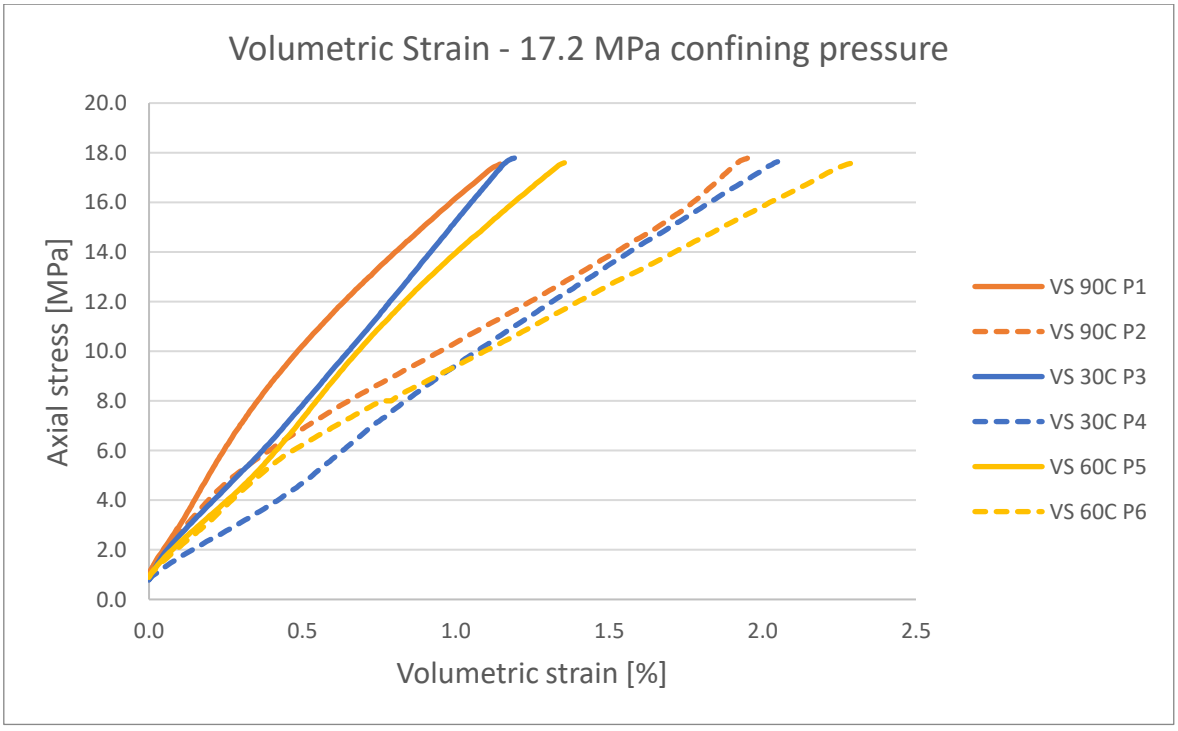

Figure 4.4 - 17.2 MPa confining pressure volumetric strain

There is no visible trend on the bulk modulus or strain data, as shown in Table 4.2. Lack of consistency is observed in the bulk modulus determined with chords and the trend line method. The bulk modulus determined with the secant origin–3 MPa method has a partial trend of bulk modulus increase with the increase of temperature. This trend only applies if the P3 test is not included in the analysis; hence, this statement cannot be concluded. A consistent axial and radial strain ratio is a great indicator of a representative core sample. However, as presented below, major inconsistency is observed in this parameter.

Table 4.2 - 17.2 MPa confining pressure hydrostatic loading

Sample	Tempe-rature [°C]	Confining Pressure [Mpa]	K-Modulus [Gpa] Secant Origin-3 MPa	K-Modulus [Gpa] Secant Origin-Max	K-Modulus [Gpa] Chords 5 MPa-7.5 MPa	Axial strain [%]	Radial strain [%]	Ratio axial/radial
P1	90	17.2	1.98	1.47	1.86	0.65	0.25	2.63
P2	90	17.2	1.56	0.79	0.79	1.09	0.42	2.60
P3	30	17.2	1.55	1.43	1.38	0.80	0.19	4.27
P4	30	17.2	0.75	0.84	0.99	1.05	0.50	2.08
P5	60	17.2	1.17	1.18	1.37	0.68	0.40	1.71
P6	60	17.2	1.11	0.70	0.72	1.42	0.44	3.23

4.1.1.2 Deviatoric Loading

The same issue goes for the deviatoric loading phase, where a great difference is seen in data collected from corresponding tests, as shown in Figure 4.5.

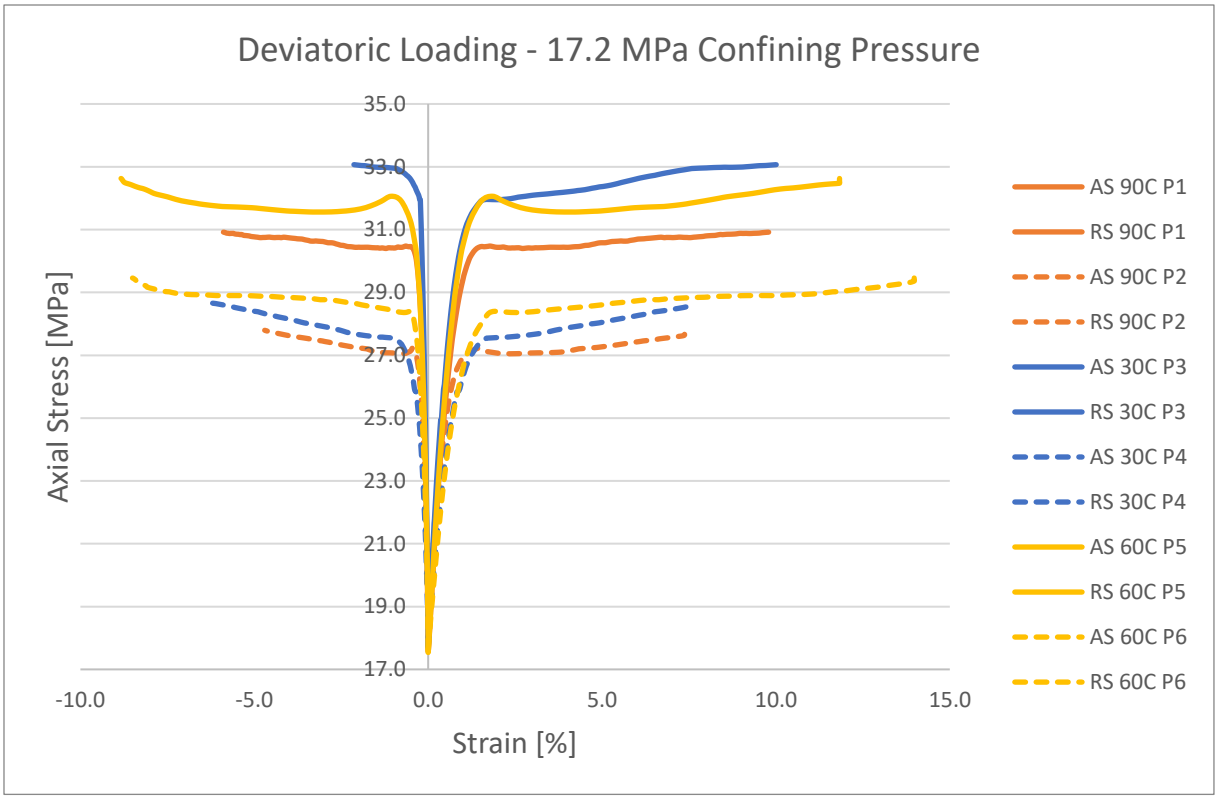

Figure 4.5 - 17.2MPa confining pressure deviatoric loading

No temperature trend is observed in either 0.2% offset yield strength or peak stress due to the high data inconsistency. Furthermore, the corresponding samples tested at 30°C have Young's modulus difference of factor 1.74, making it difficult to detect the effect of temperature. The Poison's ratio also suffers from poor repeatability as corresponding tests of P1&P2 and P3&P4 have a difference of factor 1.41 and 1.52, respectively, as shown in Table 4.3.

Table 4.3 - 17.2 MPa confining deviatoric loading

Sample	Temperature [°C]	Confining Pressure [MPa]	E-Modulus [GPa]	Poisson's ratio	Yield strength 0.2% offset [MPa]	Peak stress [MPa]
P1	90	17.2	1.85	0.22	28	30.5
P2	90	17.2	1.67	0.31	26	27.4
P3	30	17.2	2.24	0.23	28.5	31.9
P4	30	17.2	1.29	0.35	26	27.6
P5	60	17.2	1.57	0.18	29	32
P6	60	17.2	1.22	0.20	26	28.4

4.1.2 Confining Pressure 8 MPa

After experiencing poor repeatability on tests run at 17.2 confining pressure, changes mentioned at the beginning of the chapter were made to the sample preparation procedure to achieve more reliable data. Since the water on top of the samples was removed after test P7, the sample preparation of this test is not fully optimized. Therefore the P7 results are unincluded in the analysis.

4.1.2.1 Hydrostatic Loading

As shown in Figure 4.6, the changes applied to the preparation procedure have resulted in a somewhat clear trend of the effect of temperature on the axial strain. P9&P10 (tested at 30°C) have the lowest axial strain, meaning less axial deformation and potentially stronger core samples compared to tests run at 60°C and 90°C. The test run at 60°C (P8) shows a higher axial strain than corresponding tests at 90°C (P11&P12).

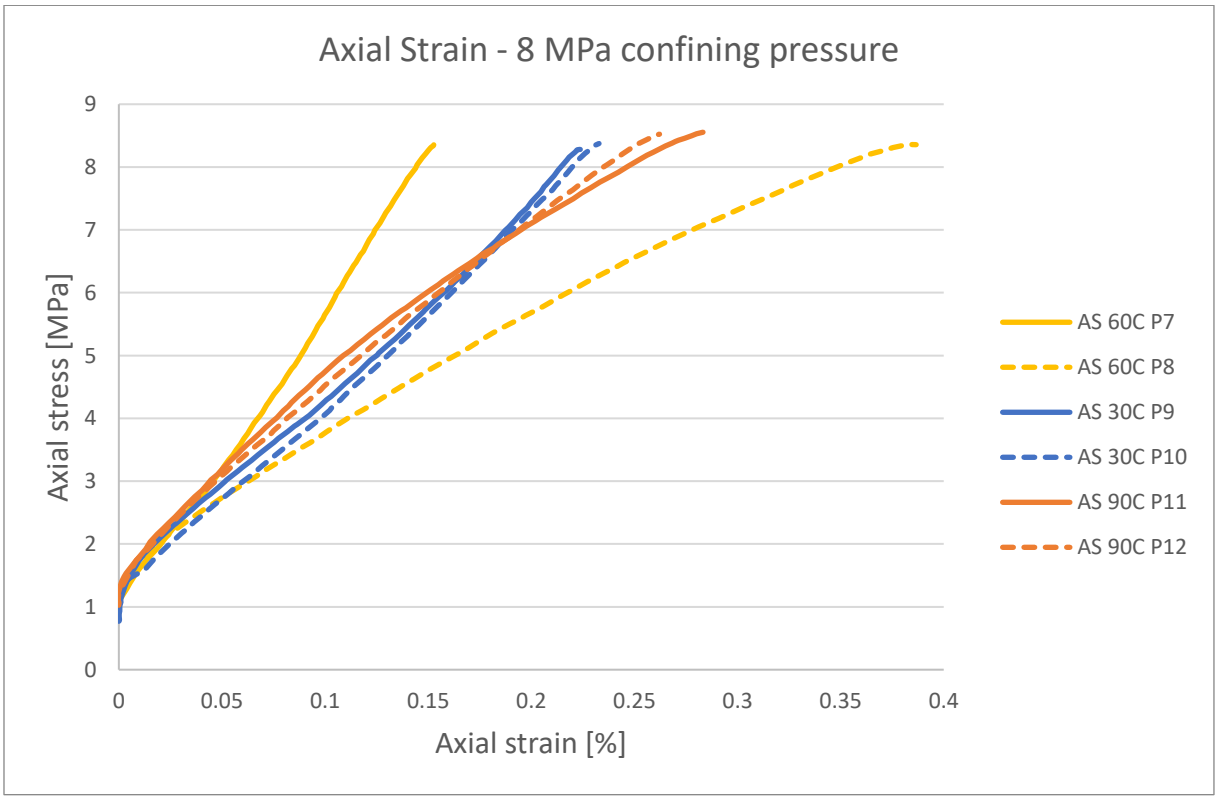

Figure 4.6 - 8 MPa confining pressure axial strain hydrostatic loading

The radial strain shows a poor temperature trend, as shown in Figure 4.7. However, if hydrostatic loading is imagined to continue above 8 MPa, a clear temperature trend can be detected. P8 is leaning strongly towards the right, and P9&P10 have a steeper axial stress increase rate than P8 and P11&P12. Therefore, by continuing hydrostatic loading, P9&P10 (tested at 30°C) will have the lowest strain percentage. Furthermore, the core tested at 60°C

(P8) have the largest radial strain. This temperature trend corresponds to the trend observed in the axial strain.

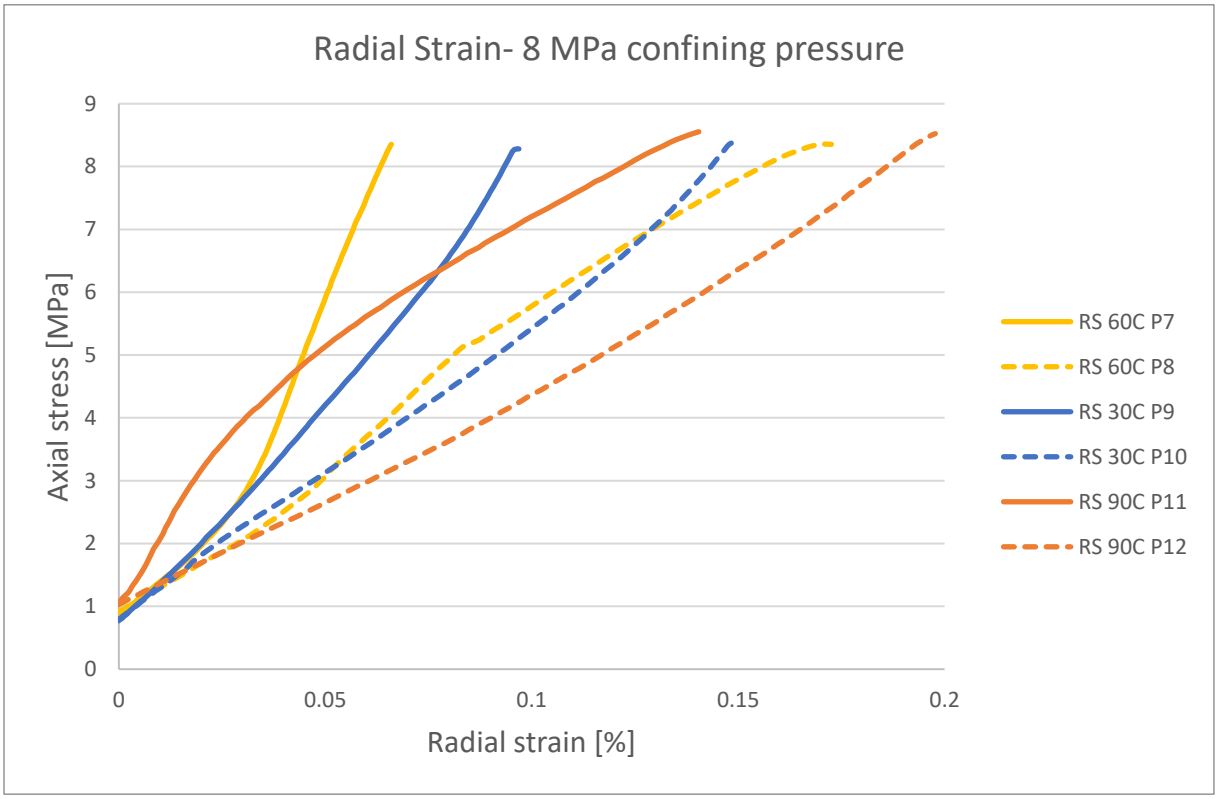

Figure 4.7 - 8 MPa confining pressure radial strain hydrostatic loading

The volumetric strain also follows the previous temperature trends at 8 MPa confining pressure, as presented in Figure 4.8. However, the trend is more visible by continuing the hydrostatic loading. P8 is strongly leaning toward the right, and P9&P10 have steep growth rates compared to other tests. This results in P9&P10 (tested at 30°C) being the test with the lowest volumetric strain. Similar to the axial and radial strain data, the volumetric strain of the sample tested at 60°C (P8) is the largest.

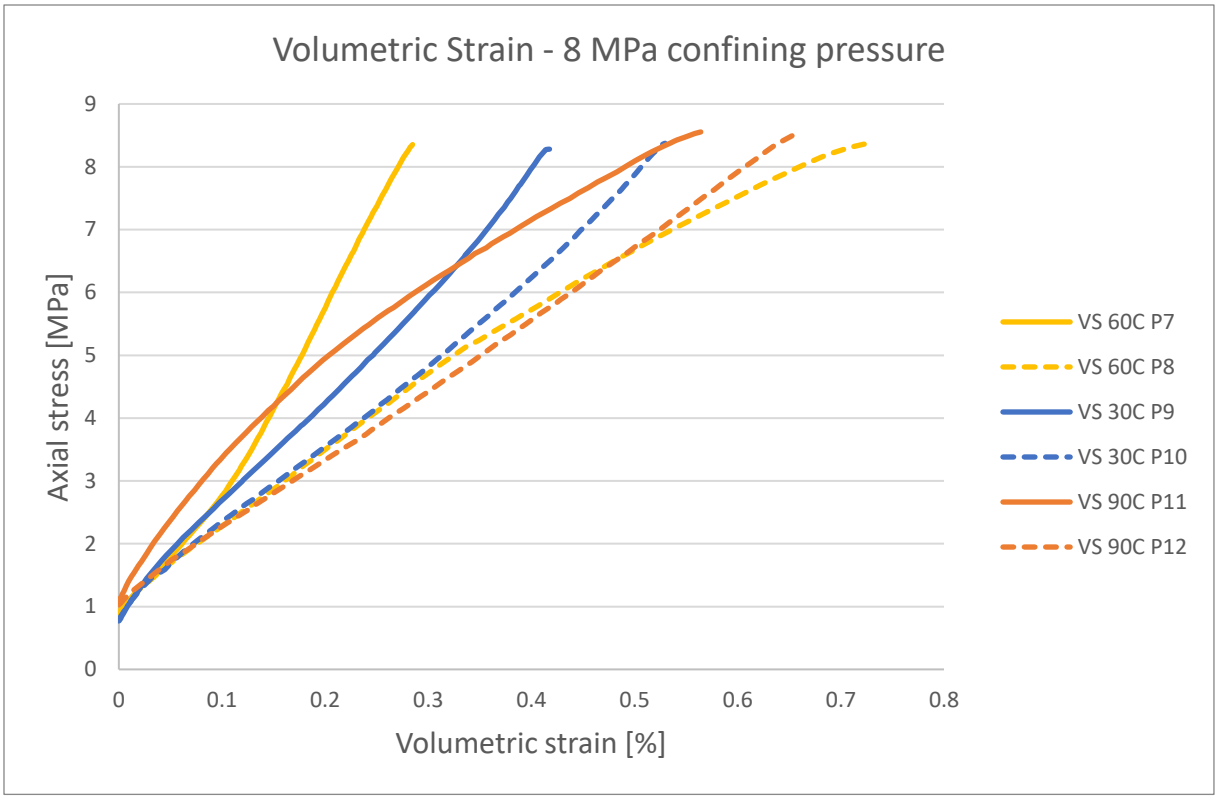

Figure 4.8 - 8 MPa confining pressure volumetric strain

As mentioned previously, the bulk modulus depends on the curve trend and method of determination. Therefore, a temperature trend is only observed on bulk modulus determined through the trend line and chords modulus method. As presented in Table 4.4, the test run at 30°C has the largest bulk modulus, while the test run at 60°C has the smallest bulk modulus value. This trend is based on not including P7, where the optimized preparation procedure was not followed. The axial and radial strain ratio shows a great improvement in consistency, confirming the positive effect of optimizing the preparation procedure.

Tablel 4.4 - 8 MPa confining pressure hydrostatic loading

Sample	Temperature [°C]	Confining Pressure [MPa]	K-Modulus [GPa] Secant origin–3 MPa	K-Modulus [GPa] Trend line origin-max	K-Modulus [GPa] Chords 5 MPa-7.5 MPa	Axial strain %	Radial strain %	Ratio axial/radial
P7	60	8	1.91	2.75	3.22	0.15	0.07	2.31
P8	60	8	1.26	1.06	0.89	0.39	0.17	2.24
P9	30	8	1.81	1.73	1.93	0.22	0.10	2.31
P10	30	8	1.37	1.37	1.55	0.23	0.15	1.57
P11	90	8	2.27	1.3	1.01	0.28	0.14	2.02
P12	90	8	1.14	1.13	1.18	0.26	0.20	1.33

4.1.2.2 Deviatoric Loading

The deviatoric loading phase reinforces the observations made on the hydrostatic loading phase. As presented in Figure 4.9, tests ran at 30°C (P9&P10) show the highest yield point of 29 MPa. The tests ran at 90°C (P11&P12) are the second strongest, while P8 (tested at 60°C) has the lowest yield point of 16.1 MPa.

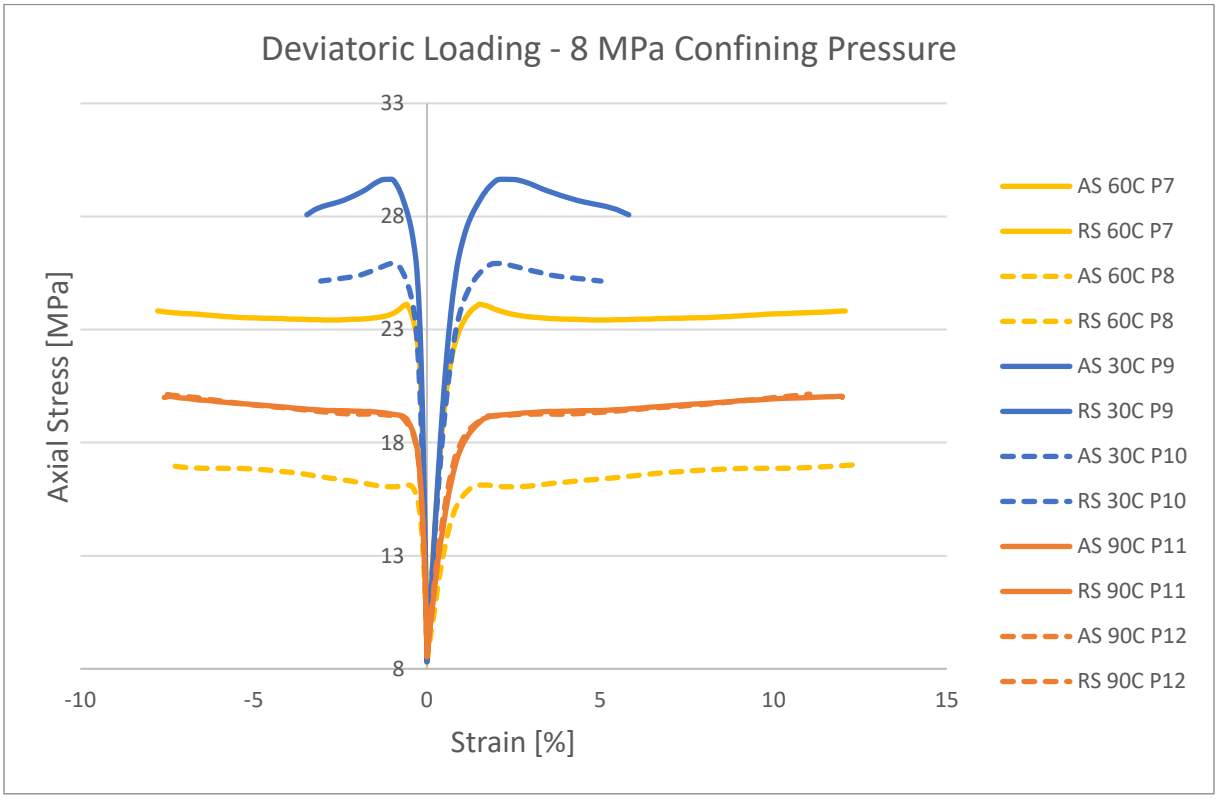

Figure 4.9 - 8 MPa confining pressure deviatoric loading

The trend also describes the ductile/brittle properties of the material at different temperatures. It is observed that tests run at 30°C are more brittle since when they reach the elastic limit, a sudden decrease is observed in the trend. On the other hand, tests run at 90°C continuous its strain hardening after reaching its elastic limit, making it more ductile.

Young's modulus also follows the trend observed in hydrostatic and deviatoric loading, reinforcing the previous observations. As presented in Table 4.5, the samples tested at 60°C shows the lowest Young's modulus at 0.99 GPa, and P9&P10 (tested at 30°C) have the highest with an average Young's modulus of 2.51 GPa. The mentioned trend is also visible in the yield strength, as shown in the table below, where the tests run at 30°C have the highest yield strength.

Table 4.5 - 8 MPa confining pressure deviatoric loading

Sample	Tempe-rature [°C]	Confining Pressure [MPa]	E-Modulus [GPa]	Poisson's ratio	Yield strength 0.2% offset [MPa]	Stress peak [MPa]
P7	60	8	2.65	0.25	21.5	24
P8	60	8	0.99	0.25	15.5	16.1
P9	30	8	2.53	0.25	26.0	29.6
P10	30	8	2.48	0.32	22.5	25.9
P11	90	8	1.27	0.24	17.5	19.2
P12	90	8	1.41	0.28	17.5	19.2

4.1.3 Confining Pressure 26 MPa

After the successful changes to the preparation procedure and achieving a somewhat clear temperature trend and repeatable results, a more reliable dataset for tests run at 26 MPa confining pressure is expected. All tests included in this dataset have had the optimized preparation procedure. The following analysis can confirm the trend observed at 8 MPa confining pressure and finalizes the true effect of temperature on the in-situ mechanical properties of granite-based geopolymer.

4.1.3.1 Hydrostatic Loading

As shown in Figure 4.10, the tests ran at 30˚C have the lowest axial strain, followed by 60˚C and 90˚C with the highest average axial strain percentage, respectively. In other words, the axial strain decreases with an increase in test temperature.

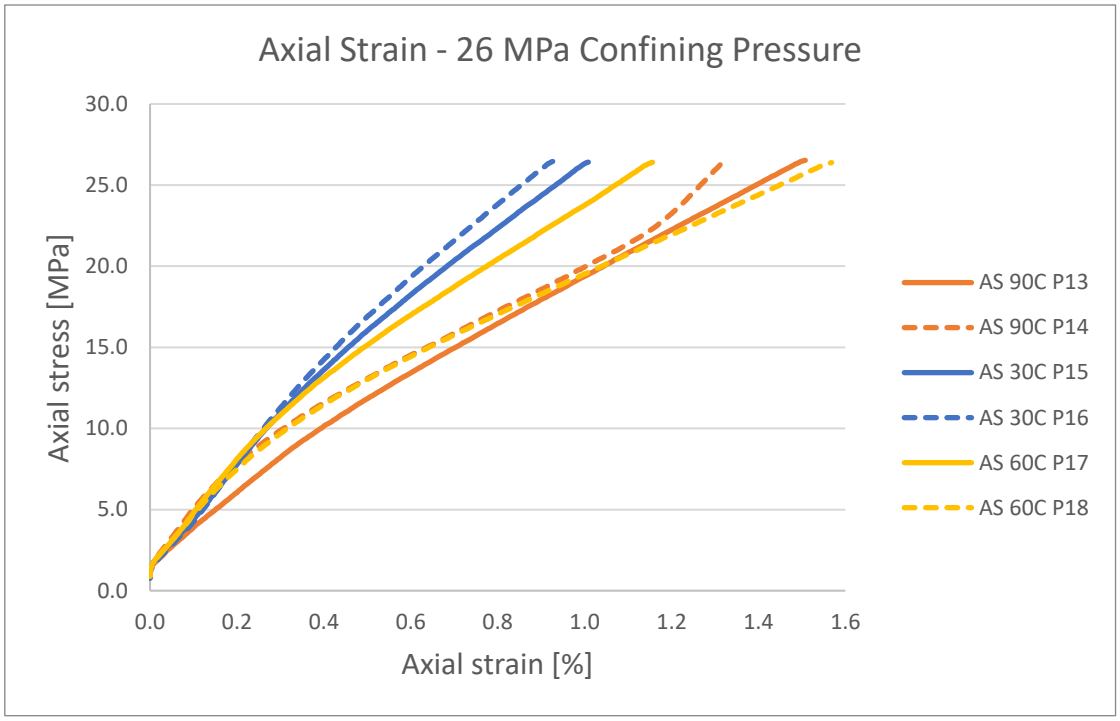

Figure 4.10 - 26 MPa confining pressure axial strain hydrostatic loading

Great repeatability is observed in tests run at 30˚C and 90 ˚C, and the results partially correspond to observations made on the axial strain. P13&P14 (tested at 90 ˚C) have the largest average radial strain, and samples tested at 30˚C have the lowest. However, P17, tested at 60˚C, has a lower strain percentage than P15&P16 and does not correspond to its corresponding test (P18). A minimized effect of temperature and lower strain difference rate is observed in Figure 4.11 compared to tests run with 8 MPa confining pressure.

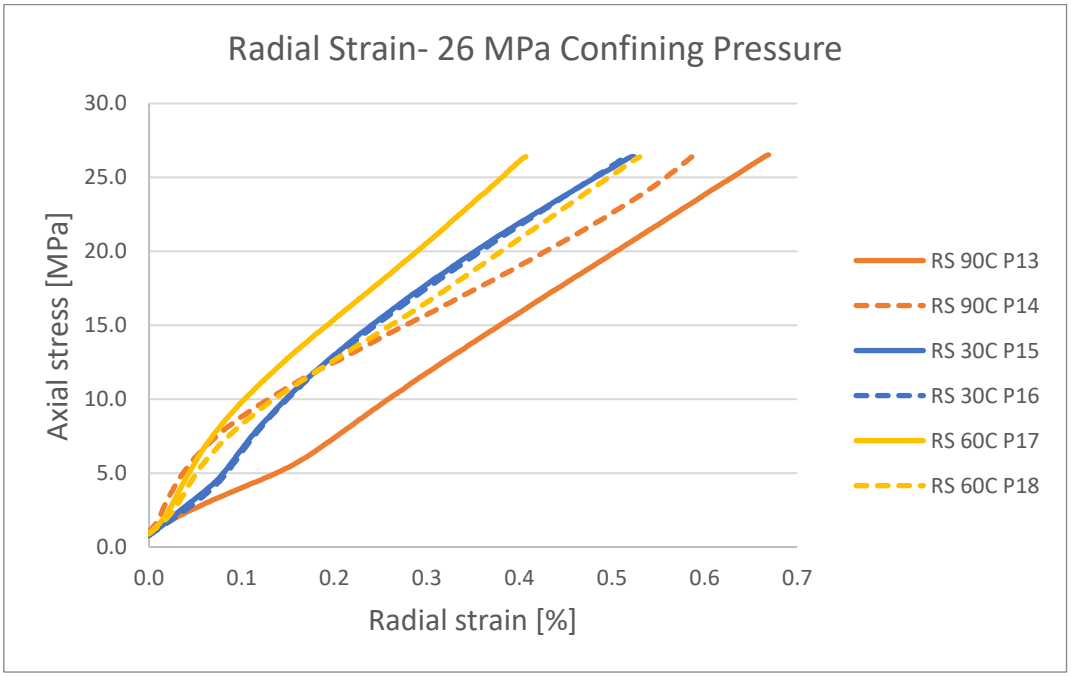

Figure 4.11 - 26 MPa confining pressure radial strain hydrostatic loading

The marginal difference in the data is also visible in the volumetric strain data, confirming the effect of confining pressure on the sensitivity of the material to temperature. P15&P16, as in previous observations, have the lowest average volumetric strain, and tests ran at 90°C (P13&P14) have the highest.

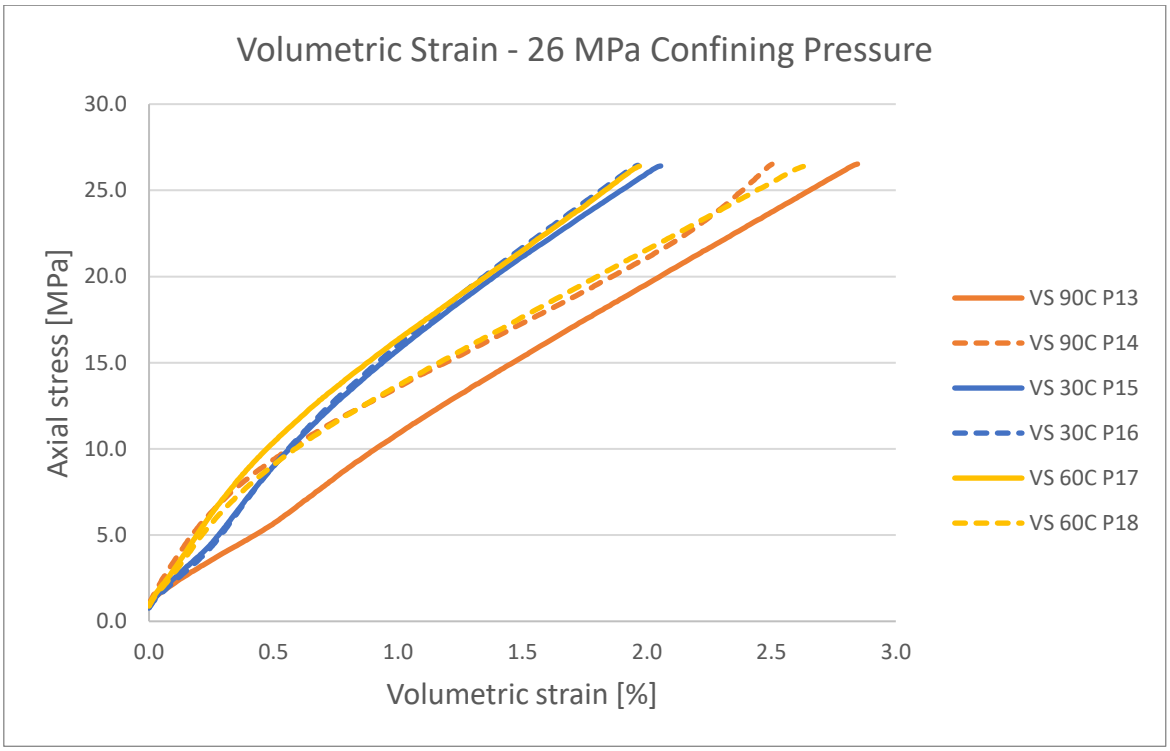

Figure 4.12 - 26 MPa confining pressure volumetric strain

As experienced with the previous set of bulk modulus data, the secant (origin-3 MPa) modulus does not replicate the true bulk modulus since most of the data have a steep strain growth at the beginning of the test. However, the bulk modulus somewhat reinforces the temperature trend detected in the test result. As shown in Table 4.6, P15&P16 have the highest trend line and chord bulk modulus, and P13&P4 have the lowest.

Table 4.6 - 26 MPa confining pressure hydrostatic loading

Sample	Tempera-ture [°C]	Confining Pressure [MPa]	K-Modulus [GPa] Secant (Origin-3 Mpa)	K-Modulus [GPa] Trend Line (Origin-max)	K-Modulus [GPa] Chord (5-7.5 MPa)	Axial strain [%]	Radial strain [%]	Ratio axial/radial
P13	90	26	1	0.9	1.07	1.51	0.67	2.25
P14	90	26	2.39	0.88	1.44	1.32	0.59	2.25
P15	30	26	1.52	1.26	1.87	1.01	0.52	1.93
P16	30	26	1.37	1.32	1.97	0.93	0.52	1.79
P17	60	26	2.05	1.25	1.91	1.16	0.41	2.84
P18	60	26	1.86	0.92	1.49	1.57	0.53	2.96

4.1.3.2 Deviatoric Loading

The results from the deviatoric loading phase reinforce the observations made from hydrostatic loading. As presented in Figure 4.13, samples tested at 30˚C have the highest average yield point of 42.9 MPa, and P13&P14, tested at 90˚C, has the lowest at 38.9 MPa. In other words, an increase in strength is observed with an increase in test temperature. Furthermore, there is less difference in the data collected from different test temperatures confirming the decrease of temperature sensitivity of the material at higher confining pressure.

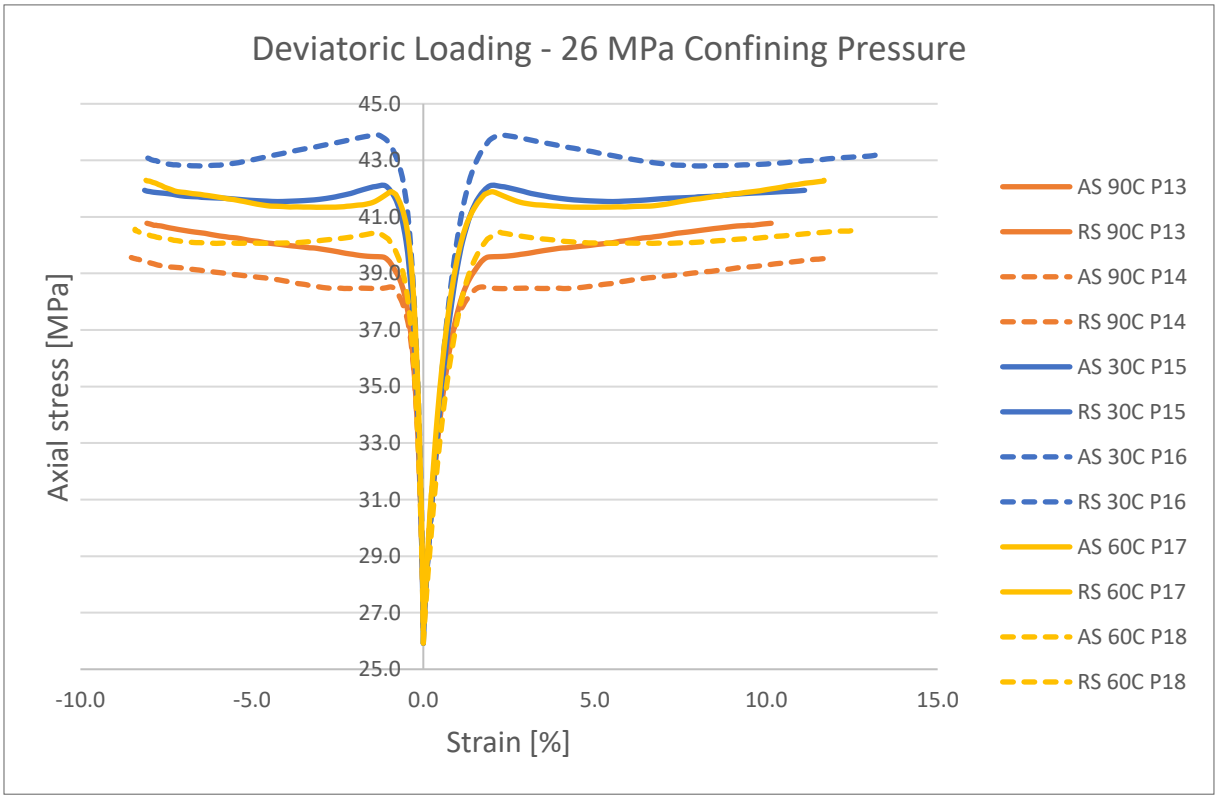

Figure 4.13 - 26MPa confining pressure deviatoric loading

Just as the observation made in the deviatoric loading at 8 MPa confining pressure, tests run at 30°C have a sudden decrease in axial stress after reaching its yield point. On the other hand, the axial stress for tests run at 90°C continues its growth after reaching yield stress toward higher ultimate strength. Hence P15&P16 are more brittle, and P13&P14 more ductile.

As shown in Table 4.7, an increase of 0.2% offset yield strength and a decrease in Poisson's ratio is observed with the increase of test temperature. However, since there is a minimized difference between P13&P18 and P17&P15, detecting a clear trend in Young's modulus is difficult.

Table 4.7 – 26 MPa confining pressure deviatoric loading

Sample	Tempe-rature [°C]	Confining Pressure [MPa]	E-Modulus [GPa]	Poisson's ratio	Yield 0.2% offset [MPa]	Peak stress [MPa]
P13	90	26	1.68	0.34	36.5	39.5
P14	90	26	1.83	0.36	36	38.3
P15	30	26	1.98	0.31	37.5	41.9
P16	30	26	1.74	0.23	40	43.9
P17	60	26	2.12	0.29	37.5	41.8
P18	60	26	1.61	0.29	34	40.4

4.2 Discussion

This chapter analyzes and discusses the effect of temperature and confining pressure on average bulk modulus, peak stress, yield strength, Young's modulus, and Poisson's ratio.

4.2.1 Effect of Temperature

The average value of each parameter is calculated and compared to detect a clear temperature trend. Due to the poor repeatability of tests run at 17.2 MPa confining pressure and P7 (8 MPa confining at 60°C), the focus of analysis is on tests run at 30°C and 90°C at 8 and 26 MPa confining pressure.

4.2.1.1 Bulk Modulus

As mentioned previously, the bulk modulus depends on the curve trend and method of determination. Therefore, a temperature trend is not detected in all three determination methods. As presented in Figure 4.14, due to the inconsistency of the initial trend of the curve, no temperature trend can be detected using the secant (origin-3 MPa) method.

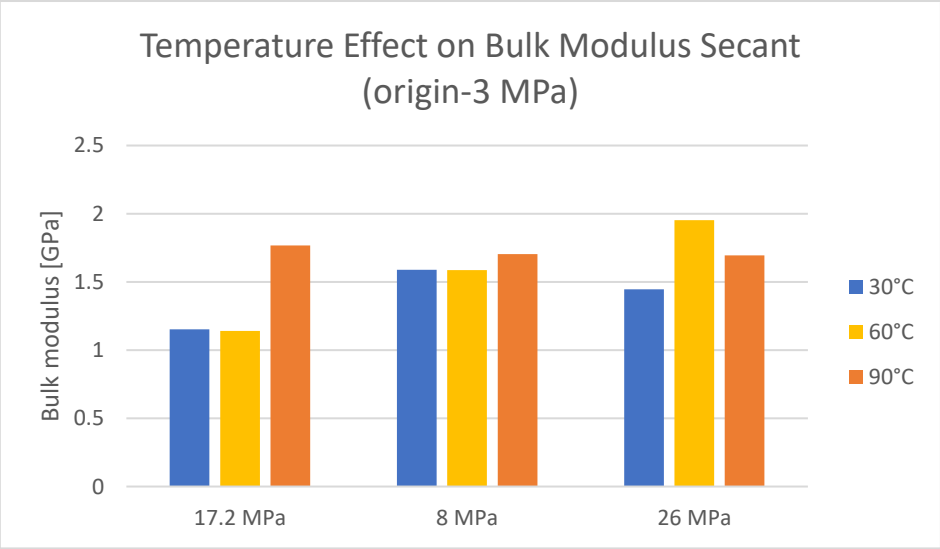

Figure 4.14 - Temperature Effect on Bulk Modulus Secant

On the other hand, a temperature trend can be detected using the chord modulus and trend line method. As presented in Figures 4.15 and 4.16, an increase in test temperature leads to a decrease in bulk modulus, resulting in a more compressible material. As mentioned at the beginning of the chapter, due to the poor repeatability of the P1-P7 test, the focus of analysis is on tests run at 30°C and 90°C at 8 and 26 MPa confining pressure.

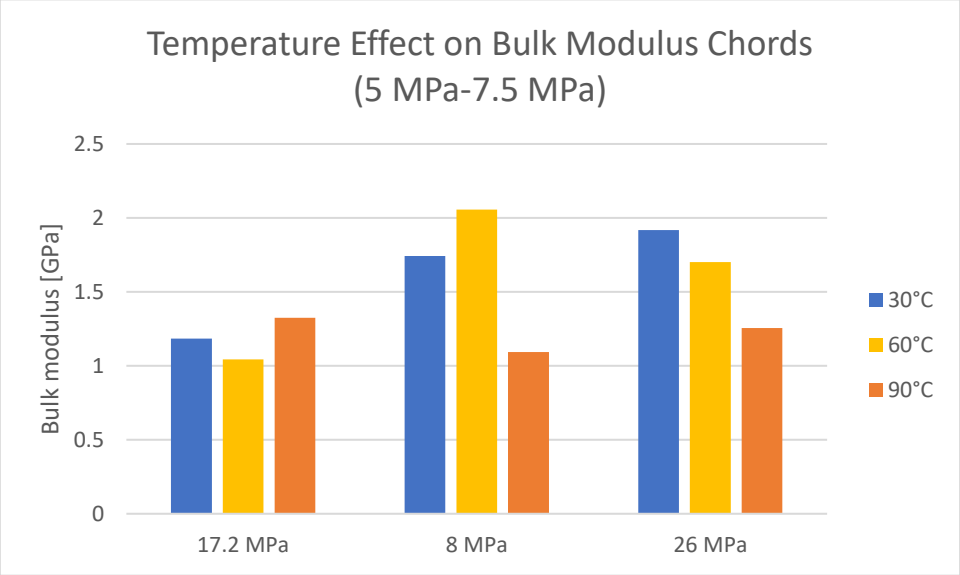

Figure 4.15 - Temperature Effect on Bulk Modulus Chords

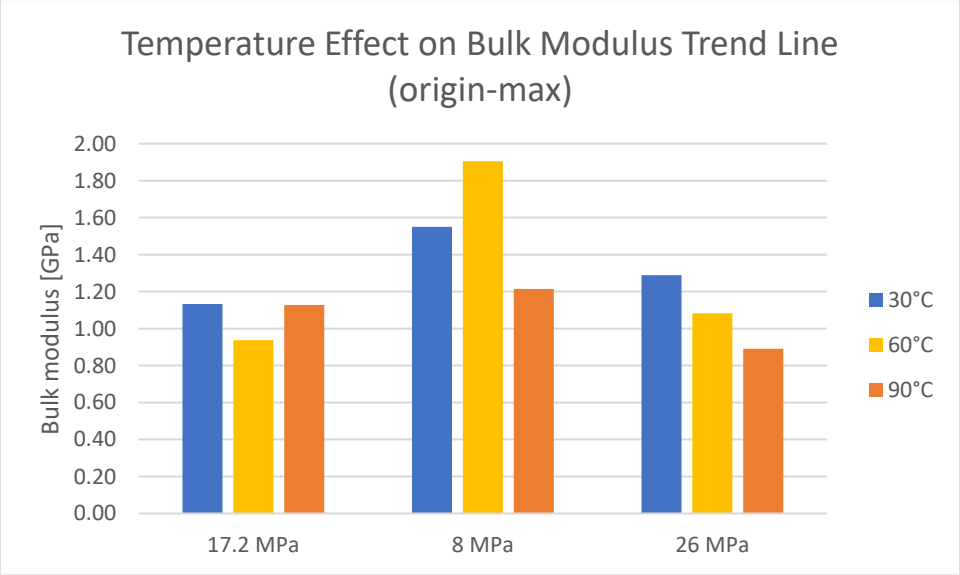

Figure 4.16 - Temperature Effect on Bulk Modulus Trend Line

4.2.1.2 Yield Strength

Both 0.2% offset yield strength and the peak stress are decreased with increased test temperature. As mentioned in Chapter 1.4, the same observation was made by Adijat et al. (2022). Another interesting observation made is the rate of change in yield strength and peak stress. As presented in Figures 4.17 and 4.18, the decrease rate in both parameters is less at 26 MPa confining pressure compared to at 8 MPa confining pressure.

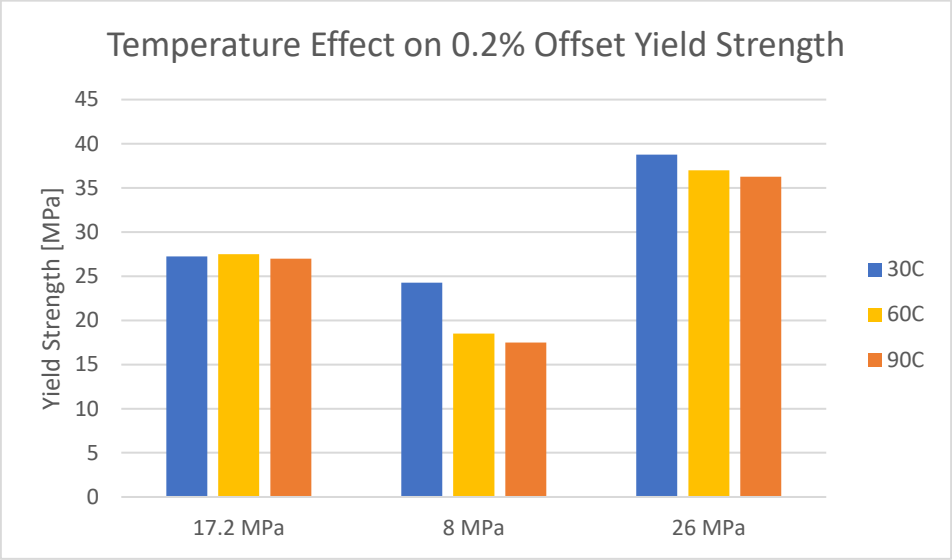

Figure 4.17 - Temperature Effect on 0.2% Offset Yield Strength

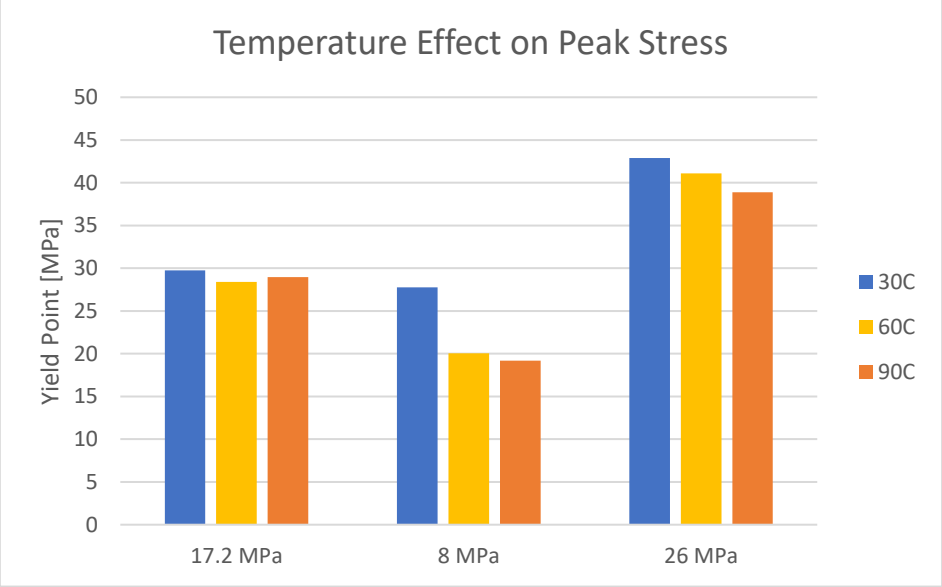

Figure 4.18 - Temperature Effect on Peak Stress

4.2.1.3 Young's Modulus

A decrease in Young's modulus is observed in both 8 and 26 MPa confining pressures; however, there is a significant difference in the rate of decline. As shown in Figure 4.19, at 8 MPa confining pressure Young's modulus decreases by 1.16 GPa, whereas on the other hand, an 0.1 GPa decrease is observed at 26 MPa confining pressure.

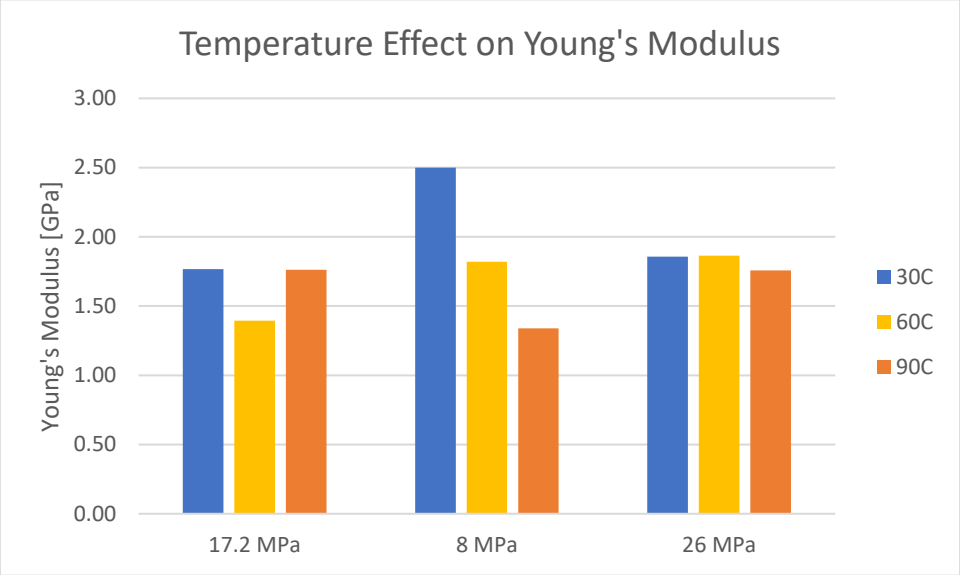

Figure 4.19 - Temperature Effect on Young's Modulus

4.2.1.4 Poisson's Ratio

Detecting a clear temperature trend on the Poisson's ratio is difficult due to material properties and test procedures. The Poisson's ratio data is determined using the radial strain data during deviatoric loading. This dataset was collected by the extensometer around the sample. The status of geopolymer samples after the triaxial test was quite different from each other as presented in Figure 4.20. Some had radial deformation on top of the sample and some in the middle. When the deformation occurs on top of the sample, the extensometer cannot detect the true deformation rate, resulting in an error in the dataset. Hence a solution for this potential error must be found in the future studies.

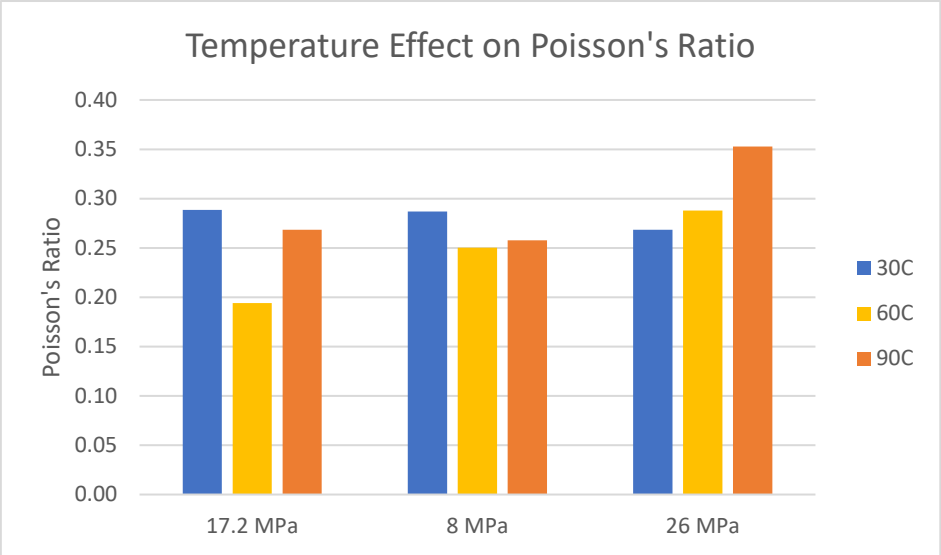

Figure 4.20 - Temperature Effect on Poisson's Ratio

4.2.2 Effect of Confining Pressure

The effect of confining pressure is analyzed on the average bulk modulus peak stress, yield strength, Young's modulus, and Poisson's ratio. Similar to the temperature trend analysis, due to the poor repeatability of tests run at 17.2 MPa confining pressure and P7 (8 MPa confining at 60°C), the focus of analysis is on tests run at 30°C and 90°C at 8 and 26 MPa confining pressure.

4.2.2.1 Bulk Modulus

As presented in the figures below, no specific effect of confining pressure on bulk modulus is observed when secant modulus (origin-3 MPa) and chords modulus (5 MPa-7.5 MPa) was used to determine the value.

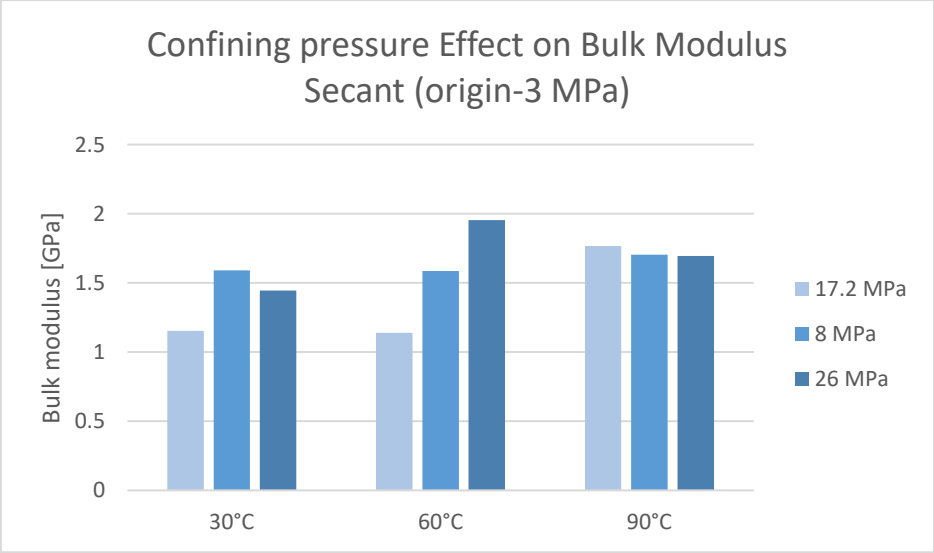

Figure 4.21 - Confining pressure Effect on Bulk Modulus Secant

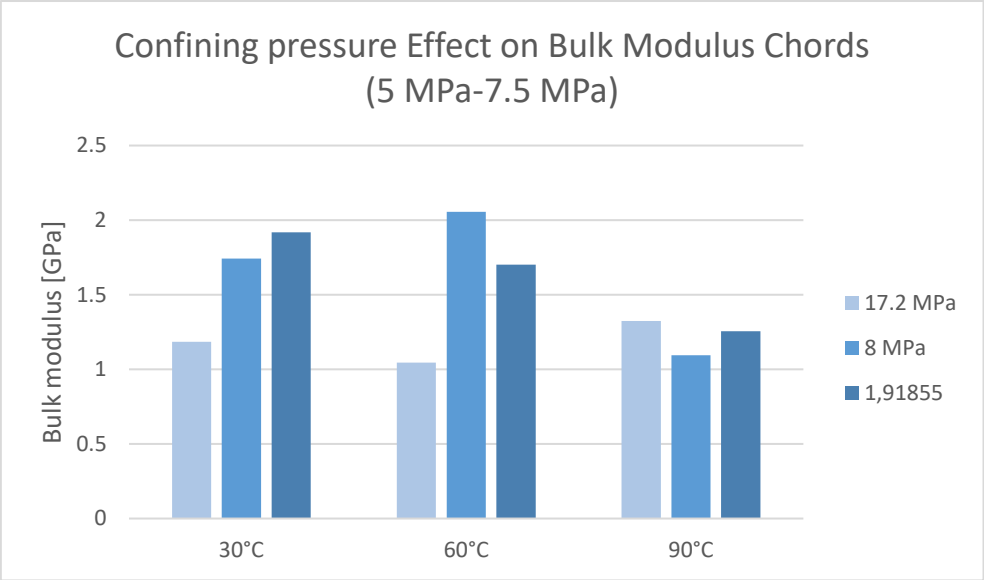

Figure 4.22 – Confining Pressure Effect on Bulk Modulus Chords

As shown in Figure 4.23, the increase in confining pressure has caused a decrease in the bulk modulus detemined with the trend line method. Since mentioned observation is relevant for only one of three determination methods, the result may be a coincidence, and therefore the statement is not concluded.

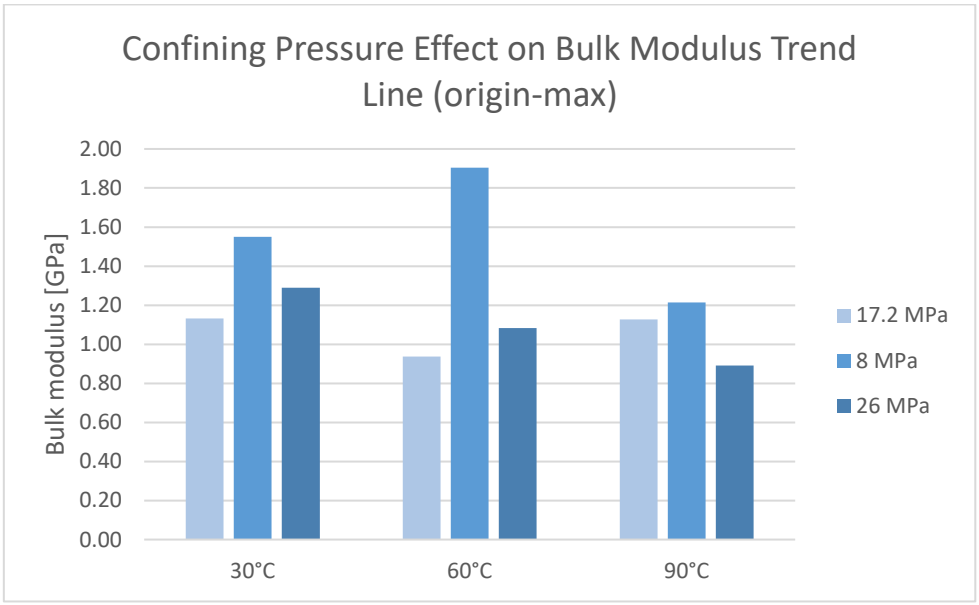

Figure 4.23 - Confining Pressure Effect on Bulk Modulus Trend Line

4.2.2.2 Yield Strength

As presented in Figure 4.24, the increase in confining pressure has resulted in an increase of 0.2% offset yield strength at 30°C by 14.5 MPa. The same effect is also observed at 60 and 90°C. At 60°C, the yield strength is increased by 17.25 MPa with increased confining pressure. Furthermore, the yield strength is increased by 18.5 MPa at 90°C.

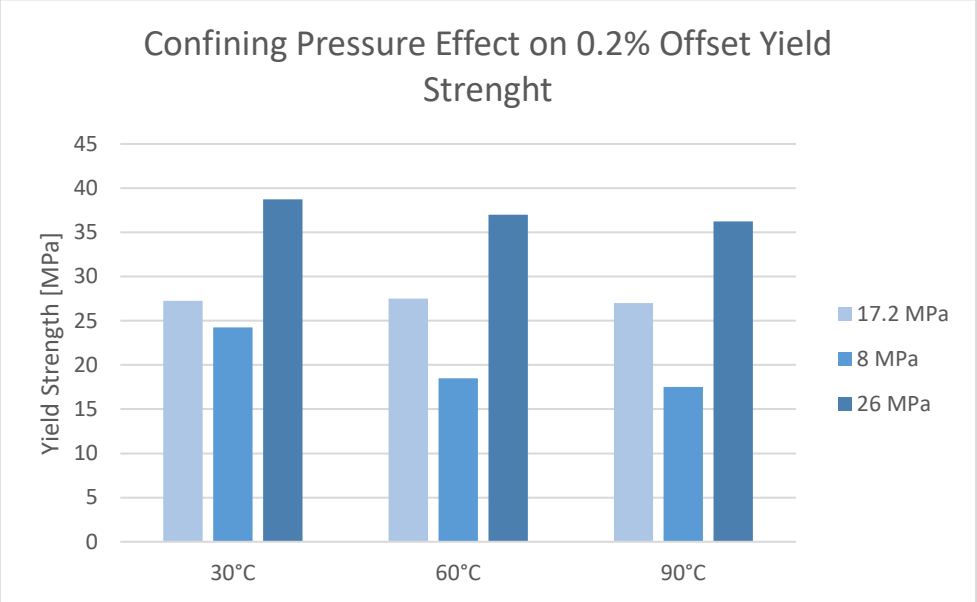

Figure 4.24 - Confining Pressure Effect on 0.2% Offset Yield Strenght

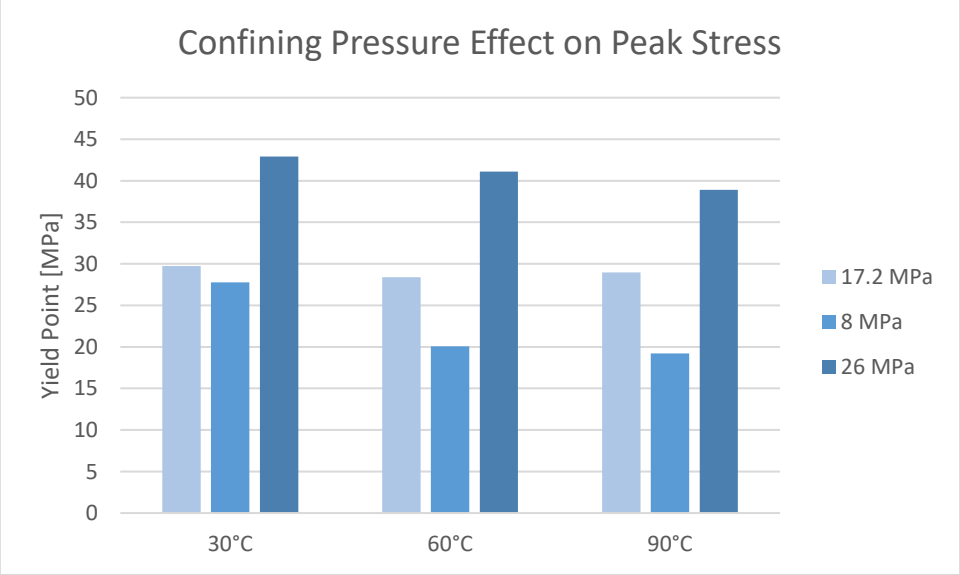

Figure 4.25 - Confining Pressure Effect on Peak Stress

4.2.2.3 Young's Modulus

As presented in Figure 4.26, Young's modulus decreases by approximately 6.2 GPa with the increase of confining pressure at 30°C. On the other hand, Young's modulus increases by 8.77 and 2.19 GPa, respectively, at 60°C and 90°C. This observation can be relevant to the statement made by Jimenez et al. (2019). Since there is somewhat consistency between curing temperature (90°C) and test temperatures at 60°C and 90°C, an increase in Young's modulus is observed. However, when there is inconsistency in the curing and test temperature, Young's modulus decreases.

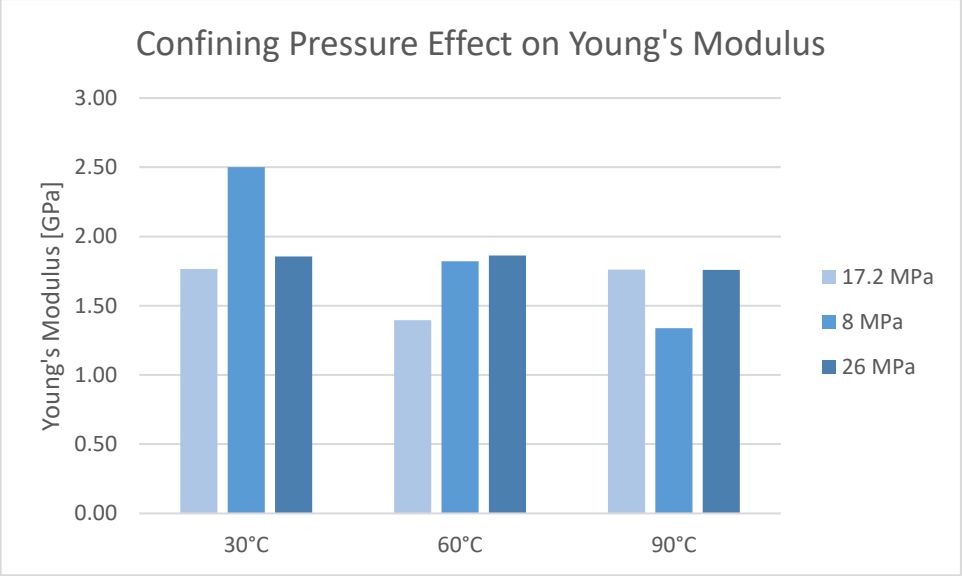

Figure 4.26 - Confining Pressure Effect on Young's Modulus

4.2.2.4 Poisson's Ratio

Similar to observations made above, the Poisson's ratio decreases at 30°C from 0.285 to 0.27 with an increase in confining pressure. On the other hand, the Poisson's ratio increases by 0.04 and 0.09, respectively, at 60 and 90°C, as presented in Figure 4.27. The following result confirms the statement by Jimenez et al. (2019) and reinforces the need for a standard cement preparation and test procedure for the industry.

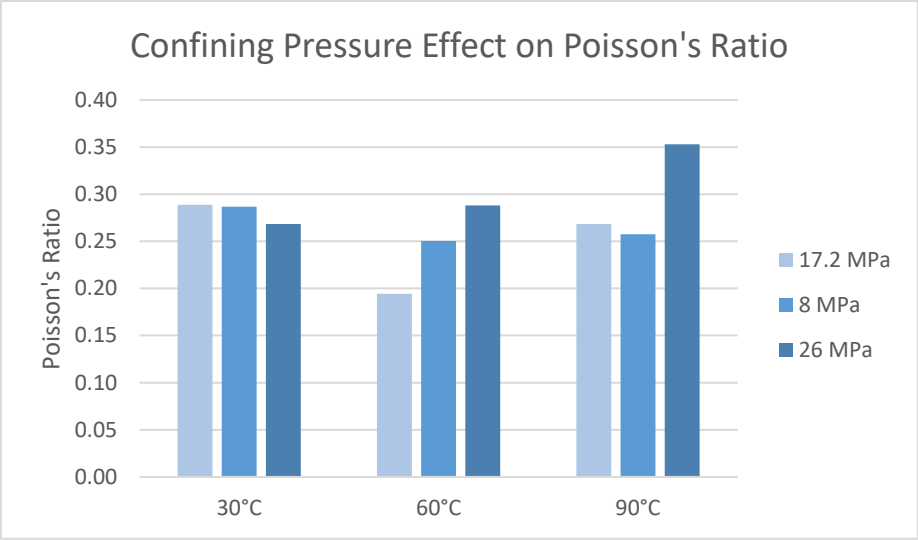

Figure 4.27 - Confining Pressure Effect on Poisson's Ratio

4.2.3 Mohr's Circle

Hence the non-representative data collected during the first six tests at 17.2 MPa, only 8 and 26 MPa confining pressure data are included in the plots. The Mohr's circle for each test temperature is presented in Figures 4.28 – 4.30. The yellow lines, also known as the failure line, are leaning toward the lower right at 30°C. This means that increasing confining pressure reduces shear stress, giving a smaller circle radius. This means that the material is more ductile, and when the material is loaded beyond its yield strength, it begins to deform plastically and ultimately experience ductile failure.

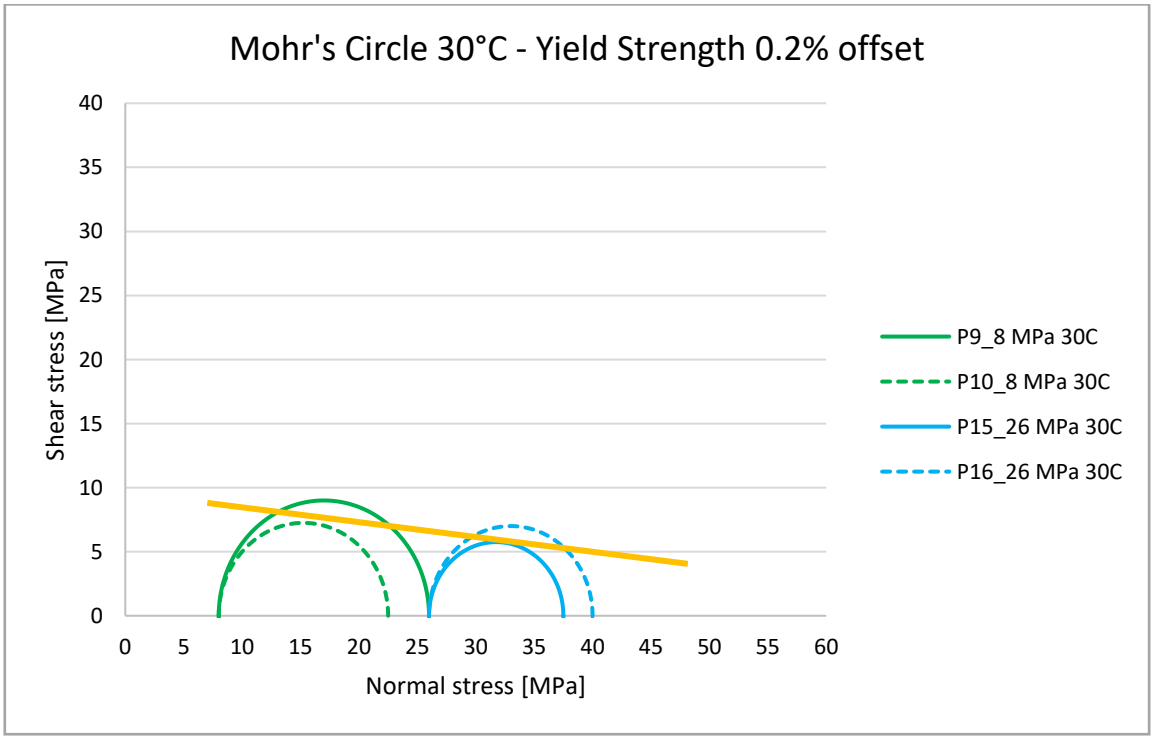

Figure 4.28 - Mohr's circle 30˚C

With an increase in test temperature (Figure 4.29 and Figure 4.30), it is observed that the failure line is firstly straightened at 60°C and later experiences a change in direction at 90°C (leaning towards the upper right). In other words, an increase in confining pressure is followed by increased shear stress and a larger radius, indicating a more brittle material. When the shear stress increases by increasing the confining pressure, the material will experience shear failure at the interaction point between the circle and the failure line. However, this does not mean that the material is only brittle and only experiences shear failure. The rate of shear stress increase with confining pressure is low, meaning that the material is still ductile. In conclusion, the material is ductile but gets more brittle at higher test temperatures.

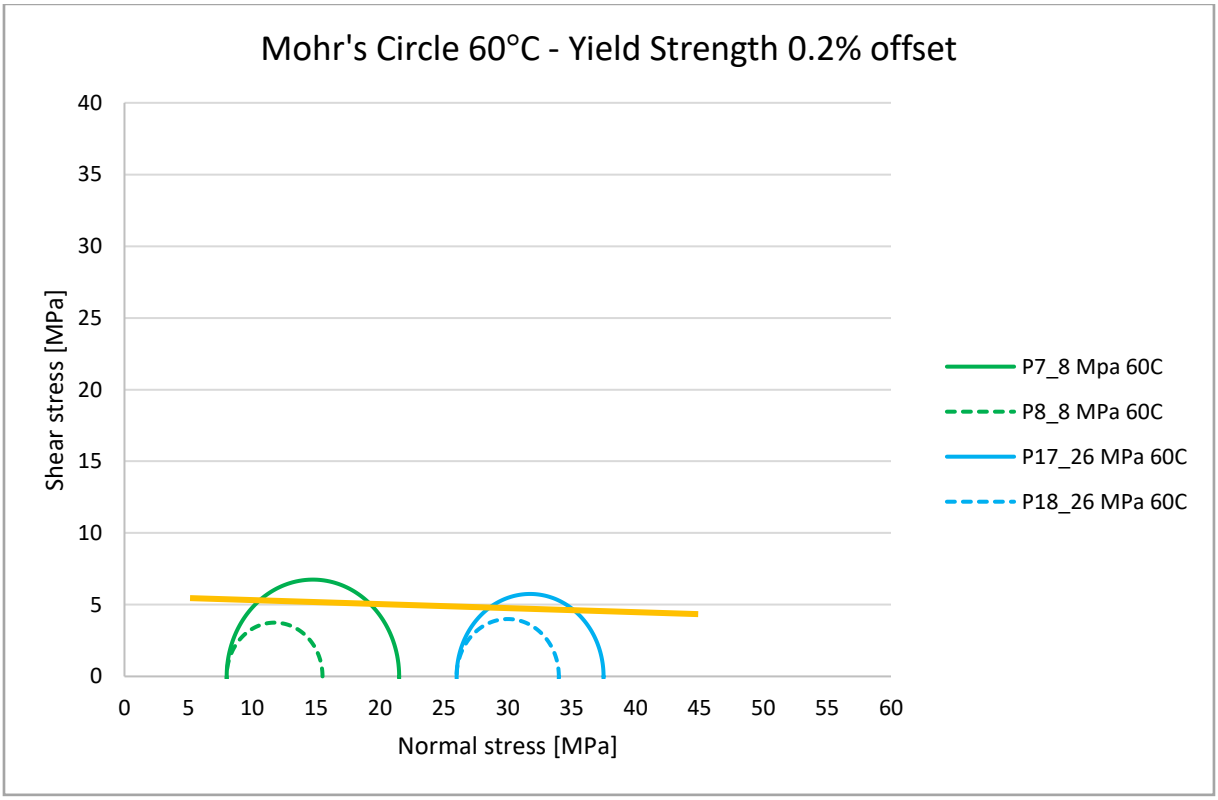

Figure 4.29 - Mohr's circle 60˚C

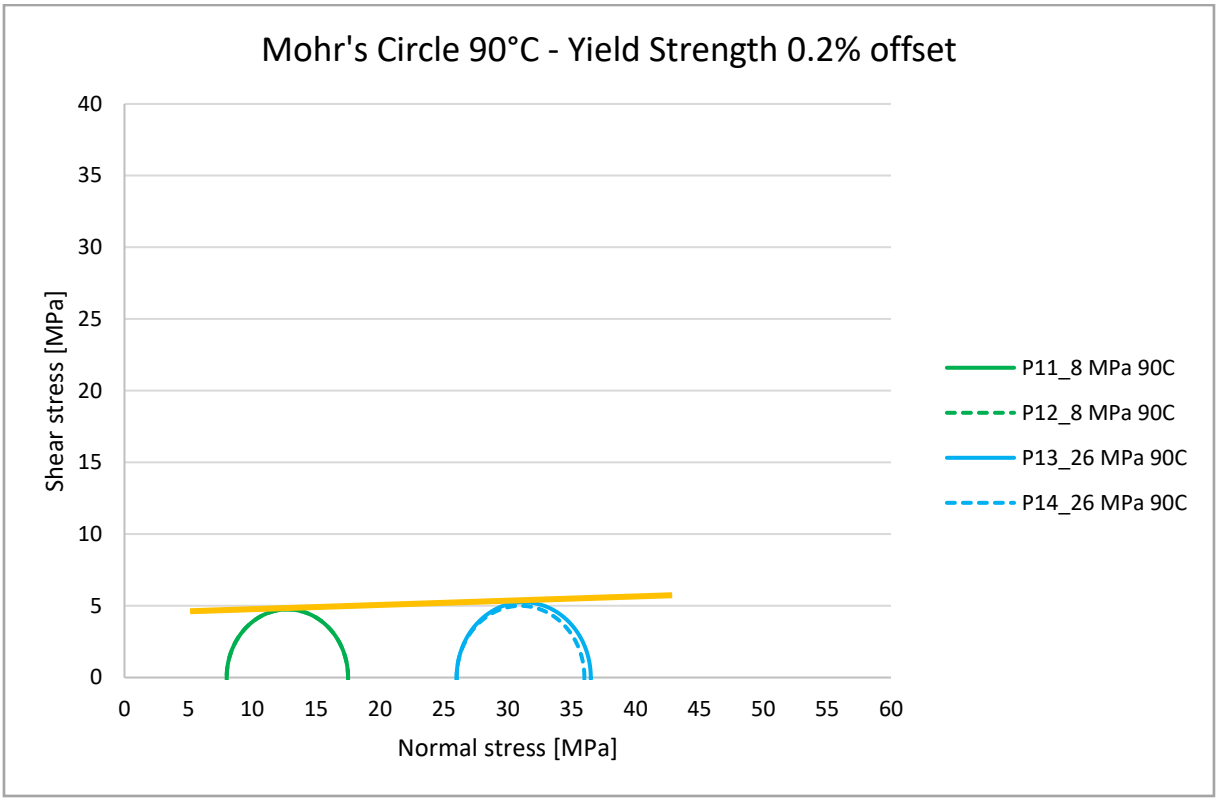

Figure 4.30 - Mohr's circle 90˚C

This statement can also be confirmed by the state of the cores after the test procedure. As shown in Figure 4.31, the cores are deformed radially and axially without experiencing shear failure at 60 and 90°C test temperature. The weight of the cores has been reduced by, on average, two grams which can confirm the ductile property of geopolymer cement.

Figure 4.31 - State of core samples after testing

It has also been observed that samples with radial expansion in the middle of the core (barrel shape) tend to have higher yield strength compared to samples with radial expansion on the top. P8 (tested at 60°C) have radial expansion on the top of the sample and yield strength of 15.5 MPa. On the other hand, P13 (tested at 90°C) is barrel-shaped after the test procedure and has a yield strength of 36.5 MPa.

4.3 Future Studies

The poor repeatability of the first six samples was followed by optimizing the preparation procedure; however, repeating those tests at 17.2 MPa confining pressure would confirm the observation made at 8 and 26 MPa confining pressure. In addition, in some analysis, havining two corresponding test was not enough and a thrid test was required for more reliable dat. Having the same test matrix done at 120C would also be interesting to analyze to see if it follows the stated trend.

An interesting observation during this study was the radial expansion on top of the samples with low yield strength. By looking at the tested core samples in Figure 4.31, it is clear that the bottom of the samples is the strongest, and the deformation occurs mostly at the top of the core. Therefore, it would be interesting to analyze the effect of height on the yield strength. In other words, a longer mold can be designed to analyze the mechanical properties of the geopolymer at different sections of that mold.

5 Conclusion

Poor repeatability was observed during the first six tests done at 17.2 MPa. Therefore, no reliable temperature trend was detected during these tests. To improve the reliability of the data, the sample preparation procedure was analyzed, and the potential stages of preparation where contamination or error could happen got detected, and a solution was applied. The stage, its concern, and its solution were as follows:

- Grease with very low viscosity and poor effect: its potential cause of contamination and poor effect damaged the samples during the removal process from the mold. The grease got changed to a red and thick HPHT Superfilm UCA grease commonly used in the oil and gas industry.
- Settlement of particles after conditioning: 30 minutes of conditioning could potentially result in settlement of particles and a non-homogeneous slurry. Since four molds are filled with one batch of a slurry mixture, the properties of the sample from the first mold would not be the same as the fourth mold. This observation was made during pouring the slurry into the molds, where the slurry had lower viscosity on the top and a higher viscosity at the bottom. To prevent such error, the slurry was slowly stirred after conditioning. In addition, the molds were marked in order such that the cores had the same positioning in the autoclave for each test.
- Water placed on top of the slurry before curing: the water is placed to accelerate the effect of pressure on the sample. However, since it is a hole on top of the molds, there is a connection between the sample and the pressure inside the autoclave. Therefore, the water was removed from the top of the slurry to avoid any potential contamination of the slurry with water.

These changes had a significant positive effect on the repeatability of the core samples. A clear temperature trend was observed in tests run at 8 MPa and 26 MPa confining pressure. The increase in test temperature resulted in a decrease in yield strength, peak stress, and Young's modulus while causing an increase in the bulk modulus. The sensitivity of the material to temperature decreases with the increase of confining pressure. The increase in confining pressure also increased yield strength and peak stress. The increase rate of these parameters got reduced at lower temperatures, potentially due to inconsistency in the curing and test temperature. Test results of the in-situ mechanical analysis are sensitive to many factors, such as curing and test temperature, curing and test pressure, length of the curing molds, and the

curing duration. Therefore, it is crucial to have a standardized test procedure for OPC and GPC in the industry where mentioned parameters and more is included.

6 References

[1] M. Khalifeh and A. Saasen, *Introduction to Permanent Plug and Abandonment of Wells*. Springer International Publishing, 2020.

[2] G. C. Bye, *Portland Cement: Composition, Production and Properties*. Thomas Telford, 1999.

[3] Z. He, X. Zhu, J. Wang, M. Mu, and Y. Wang, "Comparison of CO2 emissions from OPC and recycled cement production," *Construction and Building Materials,* vol. 211, pp. 965-973, 2019/06/30/ 2019, doi: https://doi.org/10.1016/j.conbuildmat.2019.03.289.

[4] J. Davidovits, "Geopolymer Chemistry and Applications. 4-th edition," *J. Davidovits.–Saint-Quentin, France,* 2015.

[5] J. Davidovits, "Geopolymer Cement a review 2013," pp. 1-11, 01/01 2013.

[6] M. Kamali, M. Khalifeh, A. Saasen, R. Godøy, and L. Delabroy, "Alternative Setting Materials for Primary Cementing and Zonal Isolation – Laboratory Evaluation of Rheological and Mechanical Properties," *Journal of Petroleum Science and Engineering,* p. 108455, 2021/01/27/ 2021, doi: https://doi.org/10.1016/j.petrol.2021.108455.

[7] Z. Wan, T. He, N. Chang, R. Yang, and H. Qiu, "Effect of silica fume on shrinkage of cement-based materials mixed with alkali accelerator and alkali-free accelerator," *Journal of Materials Research and Technology,* vol. 22, pp. 825-837, 2023/01/01/ 2023, doi: https://doi.org/10.1016/j.jmrt.2022.11.110.

[8] P. Nath and P. K. Sarker, "Effect of GGBFS on setting, workability and early strength properties of fly ash geopolymer concrete cured in ambient condition," *Construction and Building Materials,* vol. 66, pp. 163-171, 2014/09/15/ 2014, doi: https://doi.org/10.1016/j.conbuildmat.2014.05.080.

[9] A. A. Adam and X. X. X. Horianto, "The Effect of Temperature and Duration of Curing on the Strength of Fly Ash Based Geopolymer Mortar," *Procedia Engineering,* vol. 95, pp. 410-414, 2014/01/01/ 2014, doi: https://doi.org/10.1016/j.proeng.2014.12.199.

[10] P. Rovnaník, "Effect of curing temperature on the development of hard structure of metakaolin-based geopolymer," *Construction and Building Materials,* vol. 24, no. 7, pp. 1176-1183, 2010/07/01/ 2010, doi: https://doi.org/10.1016/j.conbuildmat.2009.12.023.

[11] M. Khalifeh, J. Todorovic, T. Vrålstad, A. Saasen, and H. Hodne, "Long-term durability of rock-based geopolymers aged at downhole conditions for oil well cementing operations," *Journal of Sustainable Cement-Based Materials,* vol. 6, pp. 1-14, 06/14 2016, doi: 10.1080/21650373.2016.1196466.

[12] E. Fjær, R. M. Holt, P. Horsrud, and A. M. Raaen, *Petroleum Related Rock Mechanics*. Elsevier Science, 2008.

[13] C. Kittel, P. McEuen, J. Wiley, and Sons, *Introduction to Solid State Physics*. John Wiley & Sons, 2015.

[14] A. Garnier, B. Fraboulet, J. Marc, and A.-P. Bois, "Characterization of Cement Systems to Ensure Cement Sheath Integrity," 04/30 2007, doi: 10.4043/18754-MS.

[15] M. Meng, L. Frash, J. W. Carey, W. Li, and N. Welch, "Measurement of Cement In-Situ Mechanical Properties with Consideration of Poroelasticity," *SPE Journal,* vol. 27, no. 05, pp. 2655-2667, 2022, doi: 10.2118/206139-pa.

[16] Y. Zheng, B. Xu, J. Pu, N. Mu, B. Wang, and M. Li, "Mechanical behaviors of cement systems in different conditions," *Natural Gas Industry B,* vol. 4, no. 3, pp. 212-216, 2017/05/01/ 2017, doi: https://doi.org/10.1016/j.ngib.2017.07.022.

[17] V. N. Lima, F. d. A. Silva, H. J. Skadsem, K. Beltrán-Jiménez, and J. K. Sunde, "Effects of confinement pressure on the mechanical behavior of an oil well cement paste," *Journal of Petroleum Science and Engineering,* vol. 208, p. 109769, 2022/01/01/ 2022, doi: https://doi.org/10.1016/j.petrol.2021.109769.

[18] Y. Li, Y. Lu, R. Ahmed, B. Han, and Y. Jin, "Nonlinear Stress-Strain Model for Confined Well Cement," (in eng), *Materials (Basel),* vol. 12, no. 16, Aug 17 2019, doi: 10.3390/ma12162626.
[19] W. C. Jimenez, R. Darbe, and X. Pang, "Enhanced Mechanical-Integrity Characterization of Oilwell Annular Sealants Under In-Situ Downhole Conditions," *SPE Journal,* vol. 24, no. 05, pp. 2308-2319, 2019, doi: 10.2118/185341-pa.
[20] A. Ogienagbon and M. Khalifeh, "Experimental Evaluation of the Effect of Temperature on the Mechanical Properties of Setting Materials for Well Integrity," *SPE Journal,* vol. 27, pp. 1-13, 04/01 2022, doi: 10.2118/209794-PA.
[21] R. Kimanzi, Y. Wu, S. Salehi, M. Mokhtari, and M. Khalifeh, "Experimental Evaluation of Geopolymer, Nano-Modified, and Neat Class H Cement by Using Diametrically Compressive Tests," *Journal of Energy Resources Technology,* vol. 142, pp. 1-15, 03/18 2020, doi: 10.1115/1.4046702.
[22] G. Kwatia, C. Ezeakacha, and S. Salehi, "Literature report of elastomer sealing materials and cement systems," *BSEE Project,* vol. 17, pp. 1-78, 2017.
[23] E. Therond, A.-P. Bois, K. Whaley, and R. Murillo, *Large Scale Testing & Modelling for Cement Zonal Isolation of Water Injection Wells*. 2016.
[24] N. Jafariesfad, M. R. Geiker, Y. Gong, P. Skalle, Z. Zhang, and J. He, "Cement sheath modification using nanomaterials for long-term zonal isolation of oil wells: Review," *Journal of Petroleum Science and Engineering,* vol. 156, pp. 662-672, 2017/07/01/ 2017, doi: https://doi.org/10.1016/j.petrol.2017.06.047.
[25] J. Sachdeva, H. Muriel, A. Nermoen, R. Korsnes, and M. V. Madland, "Chalk Surface Area Evolution during Flow of Reactive Brines: Does Oil Play a Role?," *Energy & Fuels,* 05/09 2019, doi: 10.1021/acs.energyfuels.9b00515.